Addressing high processing temperatures in reactive melt infiltration for multiphase ceramic composites

Makurunje, Phylis; Middleburgh, Simon; Lee, Bill

Journal of the European Ceramic Society

DOI:
10.1016/j.jeurceramsoc.2022.09.002

Published: 01/02/2023

Peer reviewed version

Addressing high processing temperatures in reactive melt infiltration for multiphase ceramic composites

Phylis Makurunje*, Simon C. Middleburgh and William E. Lee

Nuclear Futures Institute, Bangor University, Bangor, Gwynedd, LL57 1UT, United Kingdom

*Corresponding author:
E-mail: p.makurunje@bangor.ac.uk Tel: +44 1248 388 679

Abstract

Approaches for addressing the high processing temperatures required in reactive melt infiltration (RMI) processing of state-of-the-art multiphase ceramic matrix composites (CMCs) are reviewed. Ultra-high temperature ceramic composites can be realised by reactive melt infiltration of silicon, transition metals and/or alloys designed as immiscible phases, miscible phases, silicide phases and/or silicide eutectics to lower the temperature required for RMI. Whether carbides, borides or nitrides are envisaged in the resultant ceramic matrix composite, RMI presents an optimization challenge of balancing the composition of the phases incorporated and the processing temperature to be used. Current efforts aim at preparing complex and homogeneous microstructure preforms prior to RMI, minimising damage to reinforcing phases, applying rapid heating techniques, and developing *in situ* real-time monitoring systems during RMI. Future opportunities include integration of additive manufacturing and RMI, the increased use of process modelling and the application of *in situ* alongside *in operando* characterization techniques.

Outline

1 Introduction

Carbide, boride, and nitride ceramics with melting points above 3000 °C are often referred to as ultra-high temperature ceramics (UHTCs)[1,2]. The distinguished refractoriness of UHTCs is attractive for extreme environments found in aerospace and nuclear applications but is a challenge that demands high manufacturing temperatures to realise the ceramic matrix composites (CMCs) useful in these applications. One route used to make UHTC composites is reactive melt infiltration (RMI). In this technique, silicon, transition metals and/or alloys are melted and driven by capillary action into the voids of a preform at high temperatures typically 1400 °C and above. The perform usually consists of a carbon matrix that is ready to react with the molten phase as it is transported in the voids. The reaction forms carbides in the matrix previously occupied by the carbon phase. Addition of boron and/or boron carbide phases leads to boride ceramics. On the other hand, infiltrated and nitrided metal alloys lead to nitride ceramics.

Whether carbides, borides or nitrides are envisaged in the resultant ceramic matrix composite, RMI presents an optimization challenge of balancing the composition of the phases incorporated and the high processing temperature to be used. Silicon carbide has been the historically leading ceramic candidate for high temperature and oxidising environments. However, additions of Group IV-VI transition metal carbides, borides and nitrides further improve oxidation resistance and mechanical robustness of silicon carbide in applications beyond 2000 °C[3,4]. Therefore, the current preference is towards multiphase (hybrid) ceramic matrices. Multiphase ceramic matrix composites consist of at least two transition metals elements in the matrix, and the metals typically form ultra-high temperature ceramics (UHTCs). Such matrices have the benefit of complementing the thermochemical and thermomechanical performance of the various ceramic phases used. For example, carbides of Hf, Ta, Zr and Nb have melting points above 3500 °C and can be combined to form multiphase matrix systems with silicon carbide[5–8].

Multiphase carbide-boride combinations are common complementary systems to silicon carbide[9–15]. The popularity of such carbide-boride systems is attributed to their ability to form borosilicate glass which acts as an oxygen diffusion barrier up to 1600 °C in oxidising environments. Boria glass offers protection to 1100 °C[4,16] and silicate glass to 1200 °C in oxidising environments. However, the effectiveness of the glasses is a function of oxygen partial pressure which determines whether the oxidation proceeds actively or passively[17]. To improve UHTCs oxidation resistance, the scale porosity is reduced by using glass-forming compounds[3] and liquid-phase sintering dopants[18] to increase densification. Both decrease oxygen diffusion through the oxide scale. The need to combine multiphase UHTCs with C/C, C/SiC or SiC/C preforms provides an opportunity for the application of the RMI route.

Investigations on ranking the oxidation performance of UHTCs started in the early 1960s[19–21] although the term "ultra-high temperature ceramics" was only introduced in the 1980's[18]. In early work, carbides and borides of Hf, Zr, Ti, Ta, Nb, Mo and W were tested as UHTC candidate materials. The melting point of the UHTCs and the oxide compounds they form have been the primary screening criteria since then[3]. Derkewitz-Mattuck *et al.*[19] established the temperatures at which the scale ruptured on carbide UHTC surfaces in the following order HfC=ZrC>TiC>TaC>WC (at 1730, 1730, 1200, 1030 and 730 °C respectively). The borides of Group IV were considered the most desirable for UHTC applications[22] and ranked in oxidation resistance as HfB_2>ZrB_2>TiB_2 up to about 1950 °C[20]. Carbides and borides of the same species have been compared too[19,23,24]. However, for the Group IV nitrides, the oxidation resistance is in the order of TiN>HfN>ZrN[25]. Comparison of the oxidation resistance of carbides and nitrides has been demonstrated, for example for the zirconium systems by Harrison and Lee[26,27]. On the other hand, the reactive melt infiltration of multiphase metals into carbon preforms has been studied mostly for zirconium, ZrX and hafnium, HfX (X = C, B and/or N) composites. Nitrides have seen less frequent RMI processing compared to carbides and borides, however.

With performance in application environment considerations in mind, the multiphase ceramic matrix composites designer must select compositions that require achievable processing temperatures during reactive melt infiltration. The present review presents state-of-the-art multiphase composites that have been prepared by reactive melt infiltration. The different techniques of lowering the processing temperature required in reactive melt infiltration and the approaches of addressing these limitations are highlighted. The disadvantages of microstructural inhomogeneities and fibre damage, and consequential mechanical performance of RMI parameters are discussed. Solutions involving rapid heating, *in situ* characterization and *in operando* control techniques are anticipated, including future perspectives.

2 Addressing High Processing Temperatures

Four approaches can be used to make multiphase UHTC systems of at least two transition metals and/or including Si, while circumventing high infiltration temperature challenges:

2.1 Immiscible metallic systems

Approaches to immiscible metallic systems entail alloying a low melting-point immiscible transition metal to a refractory transition metal (UHTC-forming metal, M). Copper is typically mixed and/or alloyed with Group IV-VI UHTC-forming metals for this purpose to leverage the lower melting point of copper (~1064 °C) compared to the refractory metal. The approach can be viewed as utilizing molten copper as a carrier of the solid phase of the refractory metal, of which the later forms the carbide UHTC as shown in Equation (1). Composites that have been prepared using this approach are shown in Table 1. This approach enables RMI at temperatures between 1100 and 1300 °C.

$$M_2Cu(l) + 2WC(s) = 2MC(s) + 2W(s) + Cu(l) \qquad (1)$$

Cu-M systems are predominantly thermodynamically immiscible. The microstructures formed are characterized by phase immiscibility between the ceramic phase formed and the Cu. An example of the Cu-Ti system (Figure 1a) clearly shows the dramatic decrease of liquid phase temperature from potentially 5555 °C to about 3414 °C from 100 at.% to 1 at.% of W. Also, the Cu-W system presents the highest bimetallic mixing enthalpy known. In performing RMI, one can leverage the tiny liquid region between 1064 and 2583 °C. Comparing the Cu-W and Cu-Ti systems, the latter shows that infiltration can be performed at virtually any Ti content below 80 at.% at half the temperatures possible in the former system in which only W content below 5 at.% is possible.

Depending on the concentration of copper used, W and Cu grains typically disperse in the UHTC matrix formed and assume intragranular positions as shown in Figure 1(d-e). At 22-66 at. % of Zr, realization of nanodispersoids versus microdispersoids have been reported[28]. On the other hand, in a W/ZrC composite prepared by Khoee *et al.*[29], showed nanorange ZrC grains dispersed in a continuous copper phase. Co, Fe and Pd can be added to improve sintering in the Cu-W phases. The case of using Fe (Fe-W), instead of Cu (Cu-W) has shown, in the work of Camarano et al.[30], that besides limited thermochemical and mechanical performance issues, the long 3-8 h at 1450–1550 °C runs do not prove advantageous, however.

The case of the Cu-Ti system (Figure 2b) presents a different case from most of the refractory transition metals in that mutual dissolution occurs and intermetallics form. Increasing the Ti concentration in the Cu-Ti system leads to the formation of multiple stable intermetallics (Figure 1f-g), namely Cu_4Ti, Cu_2Ti, Cu_3Ti_2, Cu_4Ti_3, CuTi, $CuTi_2$ and $CuTi_3$[31]. Such multiple phases are the major drawback of the approach as it results in nonuniform properties in the composite. On the other hand, composites can be extended to Cu-M_I-M_{II} systems as shown by Liu *et al.*[32] for the $Cu(Ti,Hf)_2$ system. In UHTC applications involving ablation, the vaporization of residual Cu can provide transpiration-cooling advantages[33]. However, the boiling point of Cu is 2595 °C at 1 bar; Cu might evaporate easily and contaminate the processing equipment.

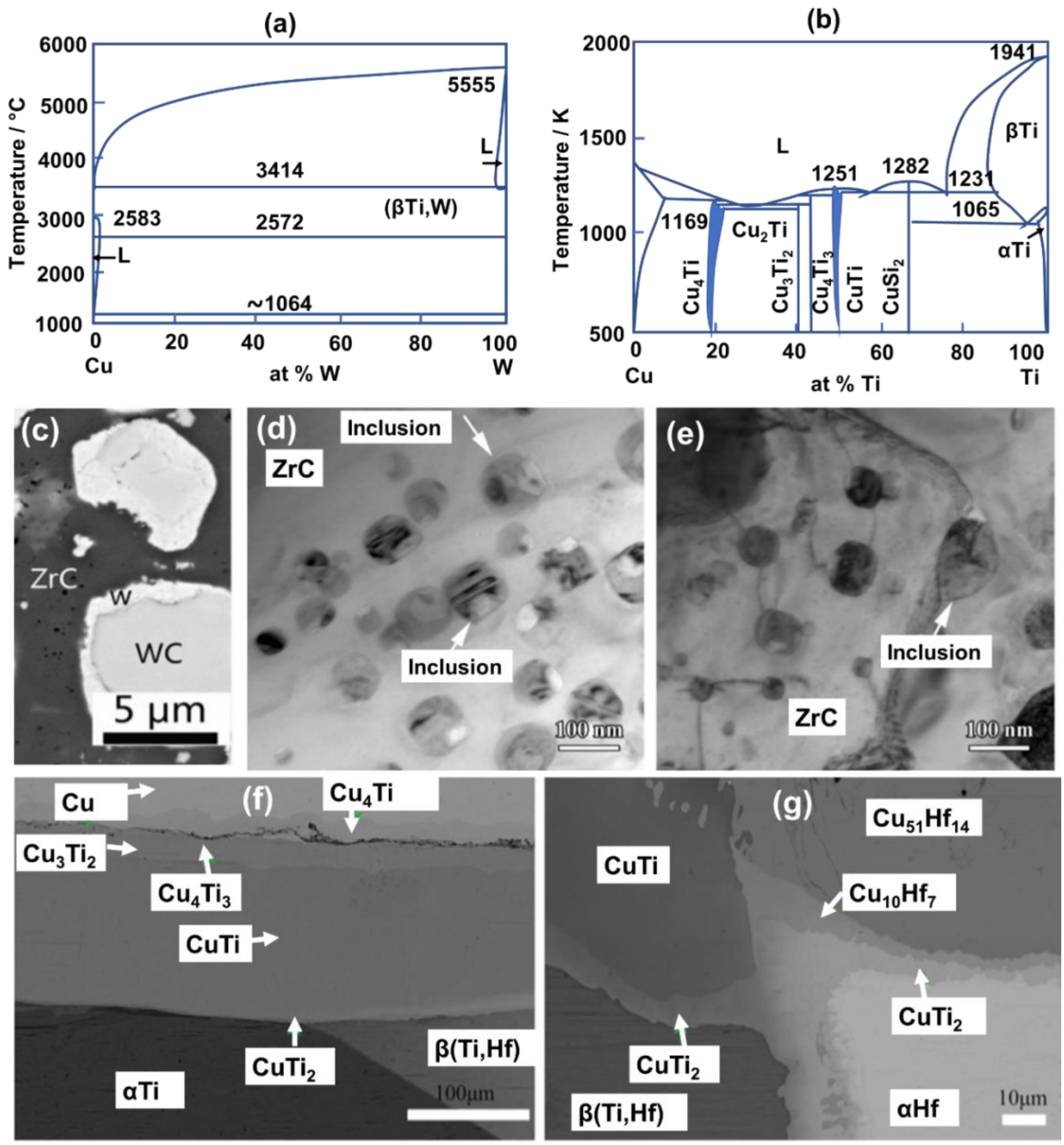

Figure 1: (a) Cu-W system[34]. (b) Cu-Ti system[35]. (c) WC-core and W-shell microstructures embedded in ZrC matrix in a WC/ZrC-Cu composite[33]. (d)-(e) W and Cu inclusions that precipitated in a ZrC matrix in a C/ZrC-W-Cu composite[28] revealing immiscibility. (f) Cu-Ti couple segment as part of Cu-Ti-Hf couple segment in (g), and the multiple intermetallics that form[32].

Although Al is a low melting temperature metal for alloying, its application has been directed at the formation of MAX phase UHTCs via RMI. Typically, Al-Ti alloys can be used for RMI, and can be extended to ternary Al-Ti-M (M = refractory metal) phases as demonstrated by Valenza *et al.*[36] who used Ti–6Al–4V titanium alloy during RMI and obtained TiC–VC and Al_4C_3 phased composite. Al potentially wets SiC when alloyed with Mo and Nb.

2.2 Miscible metallic systems

This approach combines at least two refractory metals to leverage a eutectic temperature[37,38]. The eutectic point dictates the compositions used in the infiltrant and the infiltrating temperature. This approach has been commonly used for M-Si and M_I-M_{II} alloys (M = refractory metal) as shown in Table 1.

An example is the work of Arai *et al.*[39] who used a Zr–Ti alloy to form C/C-TiC-ZrC composites infiltrating at varying Zr contents across the Zr–Ti system (Figure 2(a)). The apparent contact angle of Zr–Ti alloy with the graphite preform increased with Zr content, recording 20°, 41° and 42° for 12, 37 and 80 at. % Zr, respectively. Graded structures of SiC, $TiSi_2$ and Si phases have been reported[40,41] with the infiltrant and the reaction products forming a U-shaped profile when contacting the preform.

The reaction of Zr with C is thermodynamically more favourable than that of Ti with C, although the carbides form solid solutions in the latter system. The quasibinary ZrC-TiC system[39] shows that upon cooling the carbides, phase separation of the carbides will occur at compositions bound by binodal and spinodal lines. Combinations of metals in the infiltration process, have been studied by Zheng *et al*.[38] for the Zr-Ti system, and a number of Hf systems (HfSi, HfV, TiHf and HfMo) by Krenkel *et al.*[42]

M-Si enables a wider range of compositions to be infiltrated as shown in the Ti-Si example system in Figure 2 (b) in which multiple eutectic points are leverageable depending on whether a titanium-rich or silicon-rich composite is sought. At 1330 °C the eutectic point would solidify into $TiSi_2$ and Si; while the one at 1340 °C would solidify into β-Ti and Ti_5Si_3. Silicon contents between 15 and 60 at..% demand infiltration temperatures above 1600 °C, and above 2000 °C for Si contents in the 35-45 at.% range. An additional advantage of infiltrating M-Si alloys is less reaction exotherm temperature during SiC formation than when infiltrating Si metal[43]. Yet another advantage of infiltrating M-Si alloys is that this approach leads to formation of M disilicides, like molybdenum disilicide, which have been shown to be useful sintering and composite thermomechanical properties enhancers[43]. Of interest is how this approach would compete with the eutectic ceramics sintering technique which has been demonstrated by Nesmelov *et al.*[44] and Tu *et al.*[45] on W_2B_5–ZrB_2–SiC–B_4C and ZrC-ZrB_2-SiC composites, respectively.

2.3 Metal/ceramic-refractory silicides systems

Transition metal silicides generally have lower melting points than counterpart carbides, borides and nitrides, hence provide a low RMI temperature phase option. Silicides are further useful in introducing the oxidation-resistance enhancing silicon phase into a composite[46]. Shah[47] examined refractory MSi_2 phases that have structural applications that can potentially be used for RMI. The phase stability analysis of Wei *et al.* provides selection guidance on designing an infiltrating system for RMI[48].

Metal silicides have also been considered extensively as sintering aids[49–56]. Molybdenum and tantalum silicides are some of the most common sintering aids in UHTC composites[51–53,56]. Most studies on the effect of MSi_2 have focused on densification mechanisms in boride UHTC composites formed and their mechanical performance. Furthermore, the advantages of performing RMI with metal silicide dopings are still to be weighed against the advantages of just eutectic techniques. For example, for the TiB_2-WB_2 quasi-binary system, the eutectic temperature at 2030 °C[57] suggests that RMI should be possible at 2100 °C. Immiscibility gaps can be leveraged to sustain preferred microstructures e.g. platelet grains for mechanical performance enhancement. However, MSi_2-infiltration and sintering aids would overtake the M_IB_2-$M_{II}B_2$ eutectic infiltration approach as a large number of refractory M_IB_2-$M_{II}B_2$ systems have continuous solid solubility, e.g. CrB_2-TiB_2[57]. In addition, the eutectic-forming M_IB_2-$M_{II}B_2$ systems still would require RMI above 2000 °C.

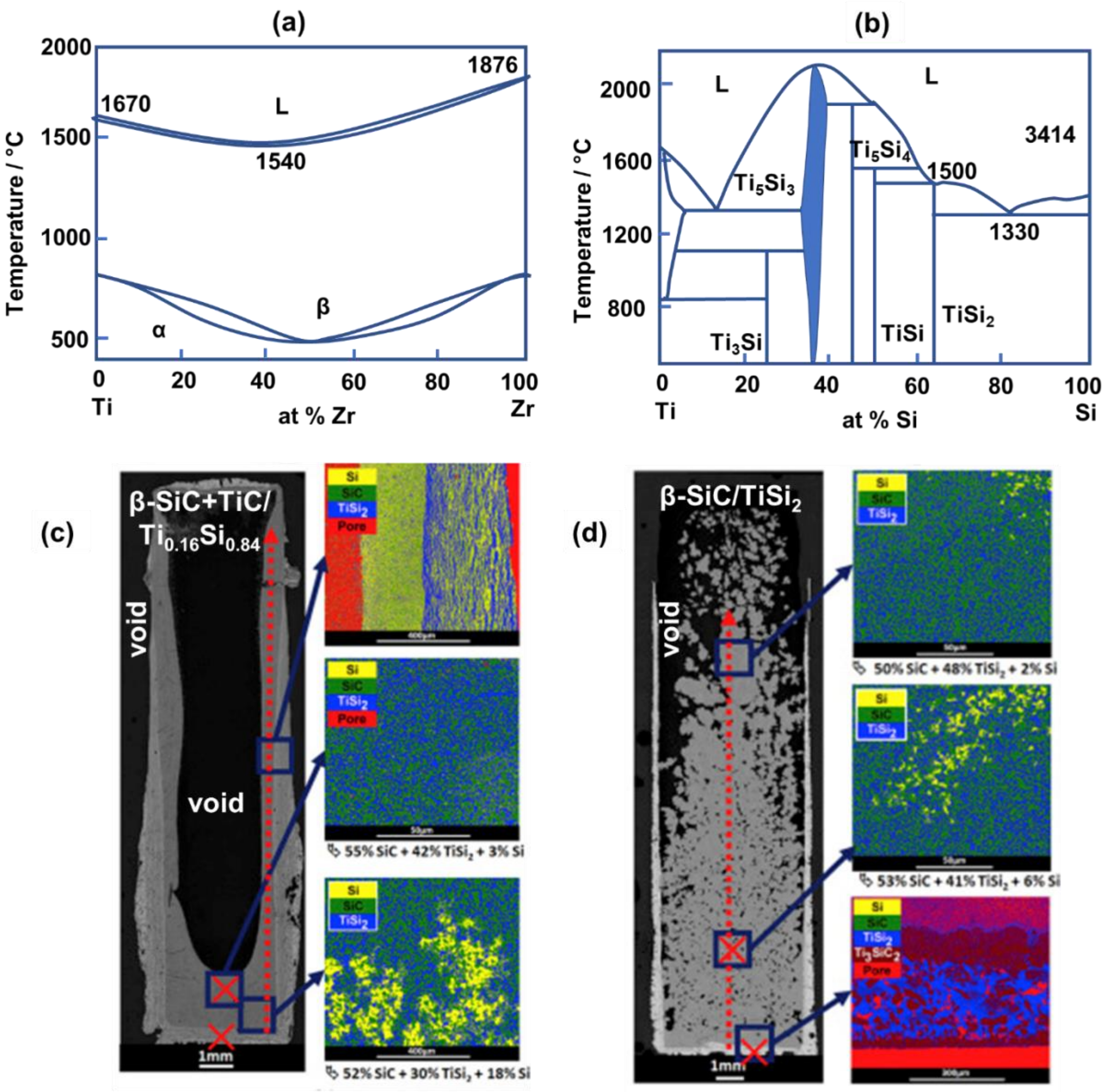

Figure 2: (a) Ti-Si system[40]. (b) Ti-Zr system[58]. Optical and phase-coloured backscattered electrons micrographs of (c) a β-SiC+TiC/ $TiSi_2$ U-profile composite obtained by infiltrating a TiC/SiC preform with eutectic $Ti_{0.16}Si_{0.84}$ alloy at 1550 °C[41], and (d) a β-SiC/$TiSi_2$ composite obtained by infiltrating a SiC preform with alloy at 1550 °C [41]. Red arrows show the infiltration direction.

$ZrSi_2$ has been demonstrated in some studies but at a lower scale than $MoSi_2$ and $TaSi_2$. Guo et al. showed that 100% theoretical density could be achieved at 1500 °C for a ZrB_2 matrix when up to 40 vol% $ZrSi_2$ is used. UHTC-forming or enhancing reactions do not occur in such a system. $TiSi_2$ has a lower melting point than most refractory but has been associated with Roger and Salles's work[40,41] showed that in the case of an α-SiC preform infiltration by Si-$TiSi_2$, a MAX phase (Ti_3SiC_2) dominated layer forms around the composite, together with $TiSi_2$ and SiC inclusions. However, when a Si-14Ti eutectic alloy was infiltrated, no MAX phases were formed albeit swelling occurred.

Meier *et al.*'s work [59] provides a guiding approach for infiltrating $MoSi_2$-Si phases into C and SiC-based preforms by including a third phase, X, which has the capability of reacting with the carbon or silicon in the system, to form infiltrated $MoSi_2$-Si-X (X = Al, B, Cr and Ti) systems. The study demonstrated how thermodynamic considerations of $MoSi_2$-Si-X systems lead to the formation of $MoSi_2$ during solidification. The system allows compositional flexibility in the composite, while ensuring that RMI can be performed at 1600 °C maximum temperature.

2.4 Refractory silicide eutectic systems

RMI of two disilicides at their eutectic composition merges the advantages of techniques (b) and (c) already discussed. As the meaning of "eutectic" ("easily melted") would have, two disilicides would be alloyed together to leverage the lowest possible melting temperature (eutectic point) in their quasibinary system during RMI. Table 3 shows examples of refractory M_I-M_{II} disilicide and penta-trisilicide quasibinary systems, and their melting and eutectic points that determine the RMI temperature to be used. It is expected that the eutectic point is lower than the melting point of the two disiliced species. However, titanium silicide is an exception; it has a lower melting point than the eutectic temperature in some cases. The Ti-Mo and W-Ti systems in Table 3 exemplify this anomaly. Furthermore, $TiSi_2$ potentially forms MAX phases[40,41] when infiltrated in reactive systems. There is a need for more thermodynamic and kinetic studies to elucidate the RMI conditions that lead to MAX phases or monocarbides when $TiSi_2$ is used as an infiltrant.

Makurunje *et al.*[46,60–62] showed the formation of UHTC composites by the RMI of two disilicides at their eutectic composition for $TaSi_2$-$TiSi_2$, $HfSi_2$-$TiSi_2$ and WSi_2-$TiSi_2$ systems. Details of such systems are shown in Table 4. Here we consider the example of a disilicides eutectic alloy in the WSi_2-$TiSi_2$ system (Figure 3(a)), and the example of a disilicide and penta-trisilicide alloy in the $(W,Mo)_5Si_3$ – $(W,Mo)Si_2$ system (Figure 3(b)). The disilicide and penta-trisilicide quasibinaries melt congruently, offering an advantage of homogeneity in the composite. However, disilicides generally have lower melting points and larger regions of thermodynamic stability than penta-trisilicides,

A 10.0W-23.3Ti-66.7Si alloy prepared by leveraging the eutectic composition of the WSi_2-$TiSi_2$ system is shown in Figure 3(c-e) in which $TiSi_2$ and $Ti_{0.6}W_{0.4}Si_2$ phases were obsserved. RMI infiltration at 2000 °C yielded the C_f/C-SiC-(Ti,W)C UHTC composite in (f-g). On the other hand, the infiltration of M_ISi_2-$M_{II}Si_2$ has made molybdenum disilicide systems favoured in the RMI process. $MoSi_2$ provides phase stability in $MoSi_2$-MSi_2 (M=Cr, V, Nb, Ta, Ti) pseudo-binary systems. Alloying molybdenum silicides with tungsten, vanadium and niobium enhances their refractory properties and the high temperature strength of the composite. Gnesin and Gnesin[63] demonstrated the infiltration of a $(W,Mo)_5Si_3$ – $(W,Mo)Si_2$ eutectic to form a coating on a C/C composite. A SiC layer was observed at the interface of the coating and the carbon substrate. In addition to carbide (W,Mo)C phases, the unreacted $(W,Mo)_5Si_3$ and eutectic phases present.

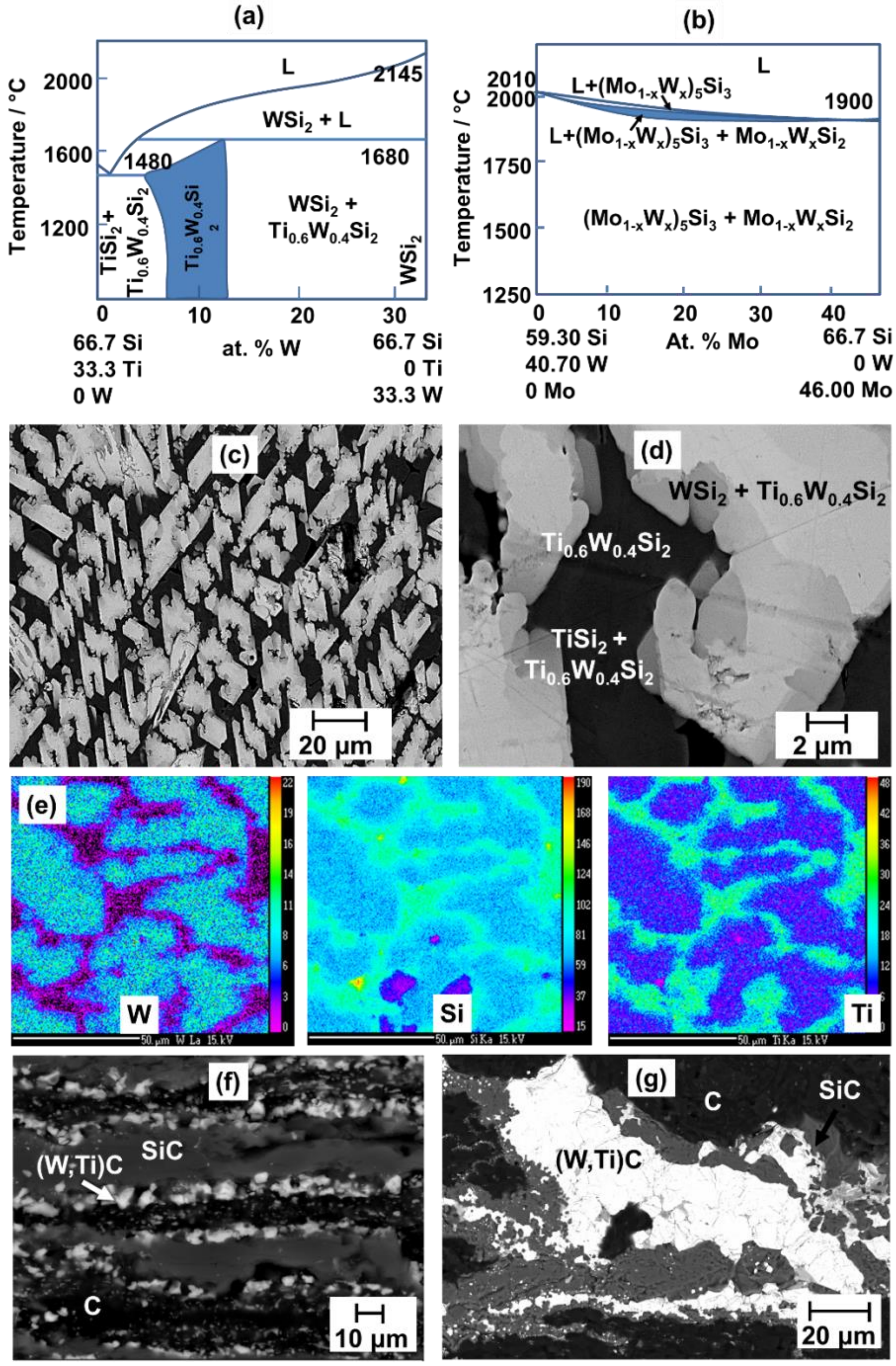

Figure 3: (a) $TiSi_2$-WSi_2 quasibinary system[64]. (b) $(W,Mo)_5Si_3$–$(W,Mo)Si_2$ quasibinary system[63]. [64](c)-(d) Microstructure of $TiSi_2$-WSi_2 eutectic alloy showing the phases defined by the $TiSi_2$-WSi_2 quasibinary system in (a)[62]. (e) EPMA elemental maps showing the $TiSi_2$-WSi_2 alloy in (c)-(d). (f)-(g) C_f/C-SiC-(Ti,W)C composite microstructure prepared from infiltrating $TiSi_2$-WSi_2 alloy into a C_f/C preform[62].

Table 1: Multiphase composites prepared by reactive melt infiltration of immiscible metal alloys

Material	Infiltrant	Technique/Equipment (atmosphere)	Dwell Temperature	Duration	Preform (Open porosity)	Comment	Ref
C/C-ZrC-Cu composite	Zr/Cu alloy, 50/50 wt %	Electric furnace (vacuum)	1300 °C	2 h	C/C preforms	Cu improves density and thermal conductivity of composite	[65]
MoC/ZrC-Cu composites	Zr-Cu alloy	tube furnace (flowing argon)	1300 °C	10 min	MoC preform (55%)	Zr reacted with the C in the MoC preform	[66]
W/ZrC composite	Zr_2Cu alloy	vacuum furnace	1300 °C	2 h	porous WC	Cu, ZrO_2, WO_2 phases in matrix	[29]
W/ZrC composite	Zr_2Cu alloy	vacuum	1300 °C	1 h	partially-carburized W powder		[67]
W/ZrC composite	Zr_2Cu alloy	vacuum	1300 °C	1 h	partially-carburized W powder		[68]
W/ZrC composite	Zr_2Cu alloy	vacuum	1200 °C	1 h	WC preform		[69]
W/ZrC composite	Zr_2Cu alloy W contents from 48 to 68 vol %	vacuum	1300 °C	1 h	partially-carburized W powder		[70]
C/C–Cu-TiC composite	Cu-Ti alloy (92-8 wt %)	vacuum	1100 °C	0.5 h	C_{NIP}/C	Cu and Cu_2O phases deterred TiC formation	[71]
W-Cu/TiC-ZrC composite	Induction smelted Zr-Cu alloy	tube furnace in vacuum	1300 °C	1 h	$(Ti_{0.75},W_{0.25})C$ (50%)	$(Ti_{0.75},W_{0.25})C$ solid solution powder	[72]
C/TiC-Ti–Cu composite	Ti-Cu alloy (50-50 wt %)	tube furnace (flowing argon)	1100 °C	0.5 h	porous starch-derived carbon (3D-printed)	TiC_x (x=0.78)	[73]

C/C-Cu_5Si-TiC composite	LSI: Si RMI: 90Cu-10Ti w/w	LSI followed by RMI (vacuum)	LSI: 1750 °C RMI: 1300 °C	LSI: 0.5 h RMI: 2 h	C_{cf}/C (37.7%) C_{cf}/C-SiC (26.7%)	5.8–6.2% residual open porosity after RMI	74

Abbreviations

C_f = continuous fibres

C_{cf} = carbon chopped fibres

C_w = carbon whiskers

C_p = particulate carbon

C_{NIP} = carbon needled integrated preform

C_{NT} = carbon nanotubes

ss = solid solution

ns = not specified

Table 2: Multiphase composites prepared by reactive melt infiltration of M-M systems and related eutectics

Material	**Infiltrant**	**Technique/Equipment (atmosphere)**	**Dwell Temperature**	**Duration**	**Preform (Open porosity)**	**Comment**	**Ref**
C/C-SiC–ZrC–TiC	80 at.%Zr–20 at.%Ti	ns	1800–2000 °C	1–3 h	C/C (ns)	$Ti_{0.82}Zr_{0.18}C_{0.92}$ phases formed	41
C/C-SiC–ZrC–TiC	35 at.%Zr–65 at.%Ti	ns	1800–2000 °C	1–3 h	C/C (ns)	$Zr_{0.83}Ti_{0.17}C_{0.92}$ $Zr_{0.57}Ti_{0.43}C$ ss phases formed	41
C/C-ZrC-SiC composites	Zr-Si alloy	tube furnace (flowing argon)	2000 °C	2h	C_f/C preforms		42
C_f/SiC-ZrC-ZrB_2 composite	Zr-B alloy	vacuum	1300 °C	1 h	C/C preform (35.23%)	Preform modified to C/ZrC composite before RMI	43
C/C-ZrTiC/SiC	16Zr-4Ti-80Si	electric furnace (argon-filled)	2000 °C	0.5 h	C_{cf}/C (~76 %)	9.7% residual open porosity after RMI	44
C/C-$Zr_{0.8}Ti_{0.2}$ C	80Zr-20Ti alloy	electric furnace (argon-filled)	1 800–2 000 °C	0.5–2 h	C_{NIP}/C (28.8 - 39.8 %)		45
C_f/C–TiC-Al-$MoSi_2$–SiC composite	63Si-23Mo-7Ti-7Al alloy	electric furnace (argon-filled)	1550 °C	6 h	C_{NIP}/C	Residual Si leads to MoSiTi phase	39
C_f/C-(Mo,Ti)Si_2-SiC composite	63Si-23Mo-14Ti 23Si-30Mo-47Ti	electric furnace (argon-filled)	1550 °C	6 h	C_{NIP}/C		46
C/C- TiC–ZrC– SiC	80Si–16Zr–4Ti alloy	electric furnace (argon-filled)	2000 °C	0.5 h	C_{NIP}/C	9.7 % residual density	47
(Hf,Zr)C-SiC coating	50Hf10Zr40Si alloy	carbon tube furnace (vacuum, 10^{-2} Pa)	1600, 1700 and 1900 °C	0.5 h	C/C composite	100, 150 and 500 µm respectively. C traces in coating	48
C/C–2HfC–2SiC–1ZrB_2	RMI: Si CVI:	tube furnace (natural gas)	1000–1100 °C	ns	C/C (~30.9 %) 7.4%	Slurry pre-infiltration, *in situ* RMI with CVI	49

C/C–2TaC–2SiC–1ZrB$_2$	RMI: Si CVI:	tube furnace (natural gas)	1000–1100 °C	ns	C/C (~30.9 %) 7.4% residual porosity	Slurry pre-infiltration, *in situ* RMI with CVI	[49]
SiC-TiC	Ti$_{0.16}$Si$_{0.84}$ alloy	vacuum furnace (5E-3 mbar)	1380-1550 °C	0.25 h	TiC-SiC (~50 %)		[40,41]
C/C-TiC-ZrC composites	Ti-12at%Zr alloy Ti-37at%Zr alloy Ti-80at%Zr alloy	vacuum furnace	1750 °C	0.25 h			[39]

Table 3: Melting and eutectic points of M_ISi_2-$M_{II}Si_2$ disilicide and penta-trisilicide quasibinary systems

M_I-M_{II}	M_ISi_2 melting point	$M_{II}Si_2$ melting point	M_ISi_2-$M_{II}Si_2$ disilicide quasibinary eutectic	$M_{I,5}Si_3$ melting point -	$M_{II,5}Si_3$ melting point	$M_{I,5}Si_3$-$M_{II,5}Si_3$ penta-trisilicide quasibinary eutectic	Ref
Ti-Ta	1490	2200	1456	-	-	-	[75]
Ti-Mo	1490	2020	~1840	-	-	-	[48]
Mo-Ta	2020	2200	~1850	-	-	-	[48]
Mo-Nb	2020	1930	1760	2100	~2450	1910	[48]
Mo-Zr	2020	1620	-	2180	~2180	-	[48]
W-Ti	2145	1490	1540	2230	2107	~1980	[64]
W-Nb	2234	2207	1860	-	-	-	[76]
W-Mo	2160	2020	Continuous solid solution	2320	2180	Continuous solid solution	[77]

Table 4: Multiphase composites prepared by reactive melt infiltration of metal silicide systems and related eutectics

Material	**Infiltrant**	**Technique/Equipment (atmosphere)**	**Temperature**	**Duration**	**Preform (Open porosity)**	**Comment**	**Ref**
C_f/SiC-ZrC-ZrB_2 composite	$ZrSi_2$ alloy	ns (vacuum)	1850∘C	ns	C_f/B_4C-C preforms	molten $ZrSi_2$ alloys into the C_f/B_4C-C preforms	[78]
C_f/SiC-ZrC-ZrB_2 composite	$ZrSi_2$ alloy	ns (vacuum)	1850∘C	ns	C_f/B_4C-C preforms	density of CMC by RMI greater than by PIP at same temperature	[79] [80]
C_f/SiC-ZrC-ZrB_2 coating	$ZrSi_2$ alloy	electric furnace (vacuum)	1800 °C	2h	C_f/C (9%), then C_f/B_4C-C preforms		[81]
C_f/SiC-ZrC-ZrB_2 composite	$ZrSi_2$ alloy	ns	1800 °C	ns	C/SiC preform (30%)	Residual $ZrSi_2$ phase in composite	[82]
C_f/SiC-ZrB_2-ZrC-Lu_2O_3	$ZrSi_2$– 5 wt % Lu_2O_3 powder	electric furnace (vacuum and static argon)	1670 °C	10 min	B_4C-infiltrated C_f/SiC prefrom (9 and 18%)	Residual $ZrSi_2$ phase with Lu_2O_3 in composite	[83]
C/C-$Zr_{0.8}Ti_{0.2}C_{0.74}B_{0.26}$	$Zr_{0.8}Ti_{0.2}$ C_{1-x}	electric furnace (argon-filled)	1 800–2 000 °C	0.5–2 h	C_{NIP}/C (39.8 % to 28.8 %)		[84]
C_f/C–TiC-$MoSi_2$–SiC composite	50Si-36$MoSi_2$-14Ti alloy	electric furnace (argon-filled)	1550 °C	6 h	C_{NIP}/C	Gradient microstructure	[85]
C_f/C-SiC-(Ti,Hf)C	$HfSi_2$-TiS_2	Crucible in spark plasm sintering furnace	2000 °C	0.5 h	C_f/C (28.3%)	BN coated fibres	[60]
C_f/C-SiC-(Ti,Ta)C	$TaSi_2$-TiS_2	Crucible in spark plasm sintering furnace	1600-1800 °C	0.5 h	C_f/C (28%)	Non-eutectic alloy composition	[46]
C_f/C-SiC-(Ti,Ta)C	$TaSi_2$-TiS_2	Crucible in spark plasm sintering furnace	1800 °C	0.5 h	C_f/C (28%)	Eutectic alloy composition	[61]

C_f/C-SiC-(Ti,W)C	WSi_2-TiS_2	Crucible in spark plasm sintering furnace	2000 °C	0.5 h	C_f/C (28.3%)	BN coated fibres	62
C/TiC-WC composite					C_{NT}		86
C_f/C–TiC-Al-$MoSi_2$–SiC composite	63Si-23Mo-7Ti-7Al alloy	electric furnace (argon-filled)	1550 °C	6 h	C_{NIP}/C	Residual Si leads to MoSiTi phase	85
C_f/(Ti,Mo)Si_2–SiC		induction tube furnace (static argon	1600 °C	0.25 h	C cloths (6-8% and (40-42%)	SiC, $MoSi_2$ and a residual $(Ti_{0.8},Mo_{0.2})Si_2$ ss	87
C/SiC-$FeSi_2$-Si	Si/5-35wt%Fe	tube under (flowing argon, 100 cm^3 /min)	1450–1550 °C	3–8 h	C_{sf}/C-binder (47%), mean pore diameter = 30 µm	$FeSi_2$ phase in matrix. Residual Si phase of <1 at. %	30
C/WC-MoC coating	(W, Mo)$_5$Si$_3$ – (W, Mo)Si_2	vacuum furnace	1950 °C	1 – 2 min	C_f/C	SiC formed, and residual silicides	63

3 Microstructural Inhomogeneities and Flaws

While multiphase systems are useful in enhancing the properties of the resultant CMC, they introduce microstructural inhomogeneities in the composite. Flaws in composites prepared by RMI exist as cracks, pores, uneven carbide grain growth, residual infiltrant “lakes” and residual carbon matrix “islands”, as well as gradient phases across the infiltrated area, as shown in Figure 4. The uniformity of the composite post-RMI primarily depends on the microstructure of the preform, particularly the homogeneity of the pore structure[88]. Simultaneous RMI phenomena to be considered are mass transfer, heat transfer and their combined effect on the matrix formation reaction[89]. However, processing conditions for each type of preform and infiltrant need optimisation. Studies[90–93] on C preforms for infiltration by Si melt highlight parameters to consider optimizing for any system, for example, porosity, pore size distribution and the reactivity of the carbon phase. Further process modelling including reaction kinetics and thermodynamics would improve our understanding of multiphase infiltrant cases.

In the case of mass transfer, the rate at which the reactants form during RMI determines if capillaries get choked with reacted product or not. Choking leads to residual infiltrant phases due to the infiltrant not percolating fully and/or not reacting fully with the preform. Choking scenarios have been modeled extensively, to predict process and material thresholds. The effects of process variables on infiltration depth (including choking) have been studied for C/SiC, SiC/SiC and other UHTC composites[94]. Besides choking, residual infiltrant phases may still be present; Suyama *et al.*[95] recorded residual phases in the range of ~12 to ~32 vol %. Residual phases may be reduced by increasing the carbon content for the reaction[95] for carbides and borides, increasing the porosity[96] or increasing the infiltration temperature[61].

Since carbide formation is exothermic,[89] temperature gradients arise in the composite during processing. Heterogeneous thermal spikes lead to thermal stresses and volume expansion changes resulting in localised cracking[97]. Temperature gradients of 170-550 ℃ have been reported in silicon carbide composites preparation[90,98]. Homogenising the preform pore structure controls the mass flow rate of the infiltrant into the preform and promotes uniform temperature profiles. Temperature-dependent composite volumetric changes in ZrB_2-based CMCs (expansion ratios between 200 and 400 vol % infiltrating at 1300 ℃ and ~120 vol % at 1500 ℃[96]), have been demonstrated as shown in Figure 4c. Hucke[99] showed that key to successful RMI is achieving the right balance between pores in the preform that are not too small to hinder capillary transport, yet not too large to reduce contact surface area therein. This ultimately reduces the thermal stresses and allows less local overheating which could lead to grain growth and silicon lake formation. Leveraging the excess heat of reaction to melting the infiltrant reduces surface tension and improves preform wetting by the infiltrant[89].

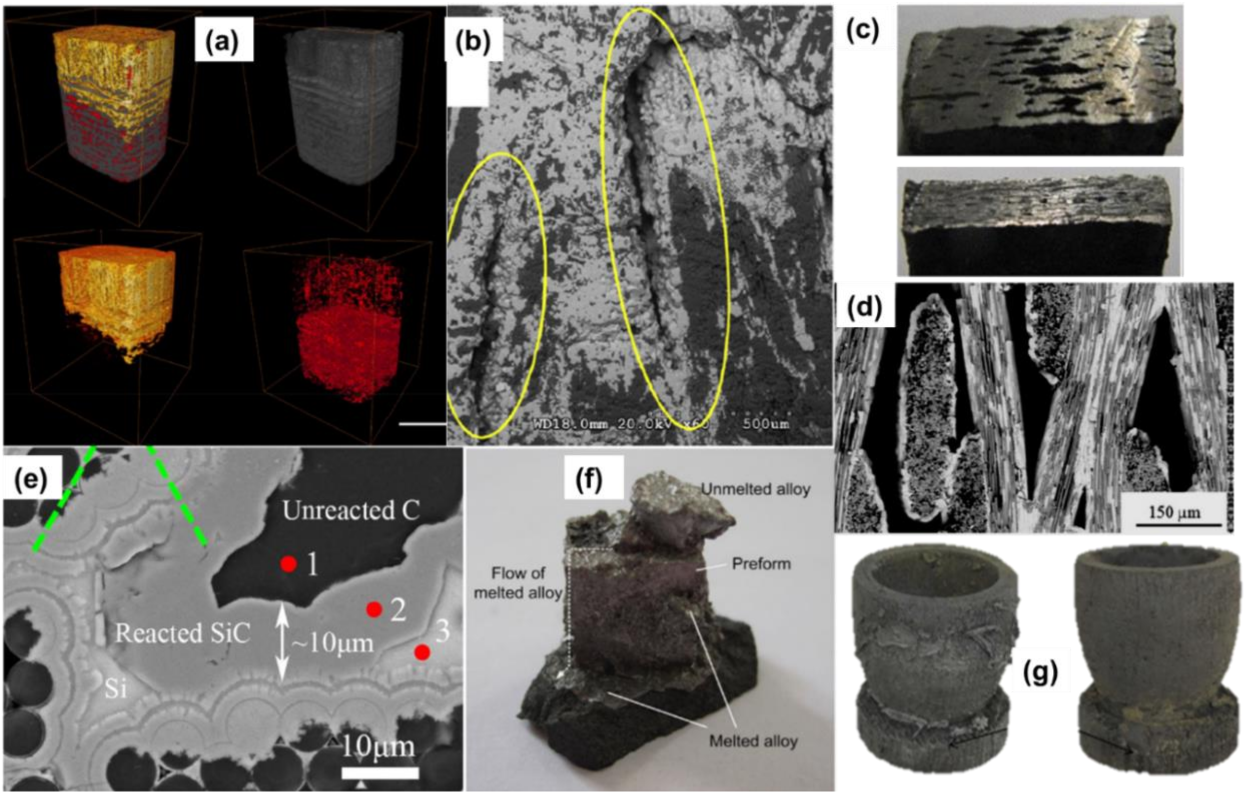

Figure 4: (a) X-ray computer-tomography of C/C-$Zr_{0.8}Ti_{0.2}C_{0.74}B_{0.26}$ showing residual porosity in red, carbon in grey and carbides in yellow[84]*. (b) Cracking in a C/SiC composite* [97]*. (c) Expansion in ZrB_2-matric composite infiltrated at 1300 °C (top) and at 1500 °C (bottom)* [96]*. (d) Spalling in a composite* [100]*. (e) Unreacted carbon and silicon phases in a C_f/SiC composite*[101]*. (f) Residual Hf alloy on a C/C preform* [102]*. (g) Residual infiltrant artefacts on a C/C–SiC composite (left) and after finishing (right)* [103].

On the other hand, the physical state of the infiltrating phase, be it powder, alloy and/or compacted pellet form, has an effect on the microstructure of the resultant composite. The impact of Zr-Si infiltrating phases on C/C preforms[104,105] is shown in Figure 5. Compacted pellets may result in a nonuniform distribution of reaction products. Alloys are typically arc-melted before infiltration; an additional step of crushing the ingots before contacting with the preform may be necessary. Alloy ingots lead to homogeneous products. Although using simply mixed (unalloyed) powders shortens the processing step, the reaction proceeds so rapidly that clogging and microstructural inhomogeneity results. Powders, alloy ingots and/or compacted pellets usually involve *in situ* melting and subsequent infiltration in an induction furnace, for instance. Alternatively, a preform dipping method allows faster infiltration (120 s) as revealed by Vinci *et al.*[106]. Automation of such a dipping system to process multiple articles is a likely opportunity for complex shaped preforms.

Understanding of RMI processes would benefit from the use of modern *in situ* characterization techniques which in future could be applied commercially *in operandi* to give improved quality assurance. Synchrotron radiation techniques have been applied for high temperature *in situ* RMI phase characterisation during e.g., of titanium and aluminide alloys[107,108]. Neutron diffraction has also been applied to the same effect with atomic disorder sensitivity e.g., on Ti-Al-Nb-Mo-B alloys alongside microscopy up to 1450 °C[109]. Laser scanning confocal microscopy, for microstructure evolution during processing, has particular capability in resolving amorphous phases evolution that are difficult for X-ray or neutron diffraction techniques[109]. Synchrotron radiation has been used with video camera aid in tracking microstructural evolution too[108]. Synchrotron radiation in situ X-Ray computer tomography has been demonstrated for flaw characterisation of C/C composites up to 1200 °C[110]. In situ mechanical properties evolution e.g., tensile strength has been demonstrated for SiC/SiC and C/SiC composites[111,112]. However, the computational processing time involved is too long, e.g., ~90 min for a scan of 1025 projection images[112].

Considering the expensive equipment required to perform both *in situ* and *in operando* characterisation techniques, simulation studies provide useful information on both the infiltration and reaction the mechanisms involved during RMI. The infiltration dynamics and reaction steps have been studied for silicon [93,113], silicon and refractory metals e.g. Zr, Ta, W and Mo[114] that can form carbides with carbon, and for silicon and non-carbon wetting metals like Cu, Co and Al[115,116]. The characteristics of the preform, the transport phenomena for the molten phases and consequential choking, the wetting of preform surfaces[115–119], and the reaction thermodynamics and kinetics across the preform, infiltrants, and reaction products.

There is opportunity for simulation studies to be extended to complex multiphase systems that involve silicon and at least two transition metals elements in the matrix.

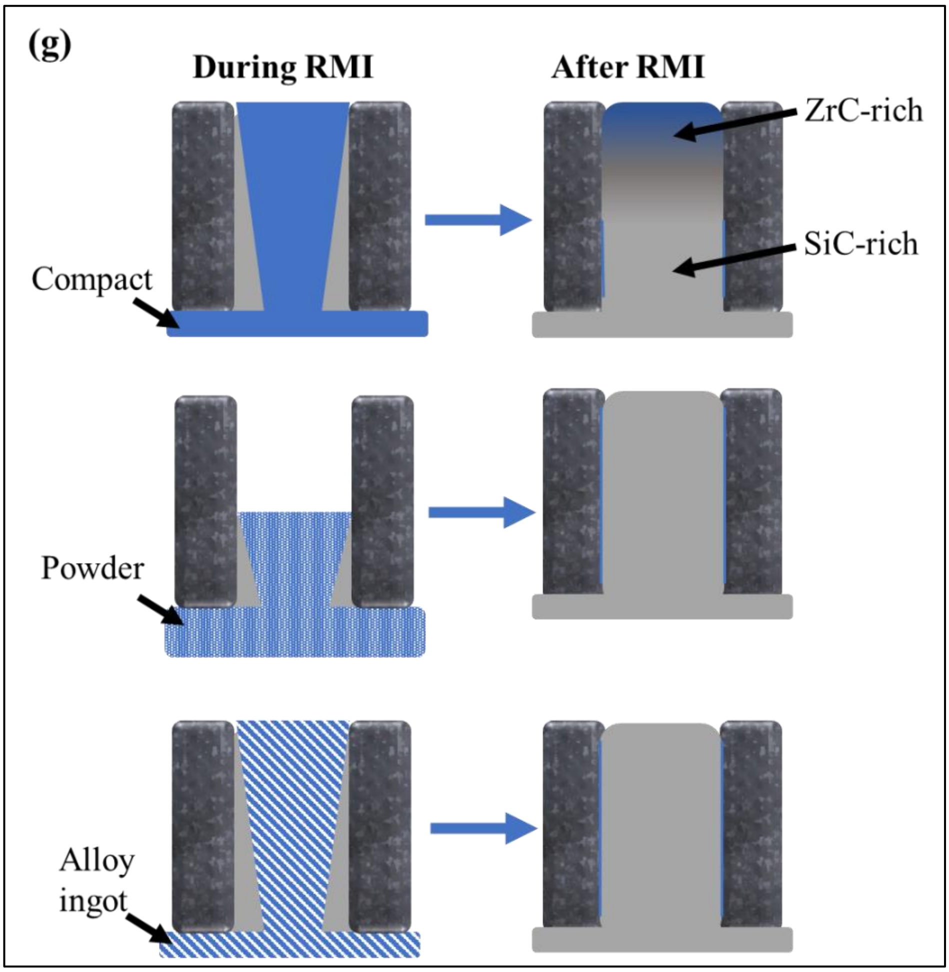

Figure 5: Schematic of the microstructural effects of using infiltrating phases in pellet, powder, and alloy forms during and after RMI of Zr-Si into C/C preforms [105].

The aforementioned *in situ* and *in operando* characterisation techniques are not readily applicable in industrial furnaces. The techniques require specialised equipment at specific synchrotron beam centres, are cost prohibitive, take long characterisation time to be part of real-time instrumentation and control suite, and usually accommodate one sample at a time. However, laser-flash techniques provide an opportunity for monitoring RMI parameters in real-time. Fraunhofer's ThermoOptical Measurement (TOM) integrated furnace system helps monitor thermophysical (e.g., infiltrant viscosity and dimensional expansion with complementary dialometers) and thermochemical (e.g., phase reactions in preform) and thermomechanical (e.g., elastic modulus and creep) dynamics[120,121].

4 Effects on Fibre Reinforcement and Mechanical Performance

During RMI, the melt has the potential to damage reinforcing phases in the composite[122,123]. The work of Tong et al.[124] showed that lengthening the infiltration process decreases the composite flexural strength. This can be attributed to fibre corrosion by the infiltrating melt as shown schematically in Figure 6(a). To protect fibres during the RMI process, barrier coatings can be introduced around them. Barrier coatings, for example pyrolytic carbon, BN[125], B_4C[126], TiB_2[127]and SiC[128], are typically introduced by chemical vapour deposition (CVD) or polymer infiltration and pyrolysis (PIP). However, when the melt reactively corrodes the interphase and/or the fibre, the latter phases fuse with the matrix to form a continuous phase limiting crack deflection and resulting in a flat fracture surface. Pre-densification of the preform matrix by less corrosive methods like room temperature slurry infiltration can also reduce the processing duration for RMI. However, cracking and delamination in the composite can be exacerbated by heat-treatment of the preform prior to RMI[129].

Bending strength studies are used to determine the robustness of the composites in distributing stress along the fibres. Fractography studies are also useful in determining the fibre pull-out as a qualitative assessment of the damage on fibres after RMI. The premise of fibre-pull out tests is that when an infiltrant is bonded with the fibres the fibres become fused to the matrix and lose their function of transferring loads. Considering the varying degrees of melt interaction with fibres, shown by the schematic in Figure 6(c-d), varying degrees of fibre pull out are observed in the fracture surfaces of the UHTC-CMCs. The differing extents of fibre pull out are also influenced by crack deflection mechanisms. The mechanism consists of fibres debonding from the matrix (Figure 6e) or form the interfacial coating (or interphase) (Figure 6f) to facilitate crack deflection. These differences give the fracture surface a jagged finish across the reinforcement orientation. Chen et al.[126] showed that the jagged microstructures can also be observed at the interfacial coating fracture surfaces. The non-uniform corrosion of fibres also promotes the formation of fibre bridges in the case of matrix failure or spallation.

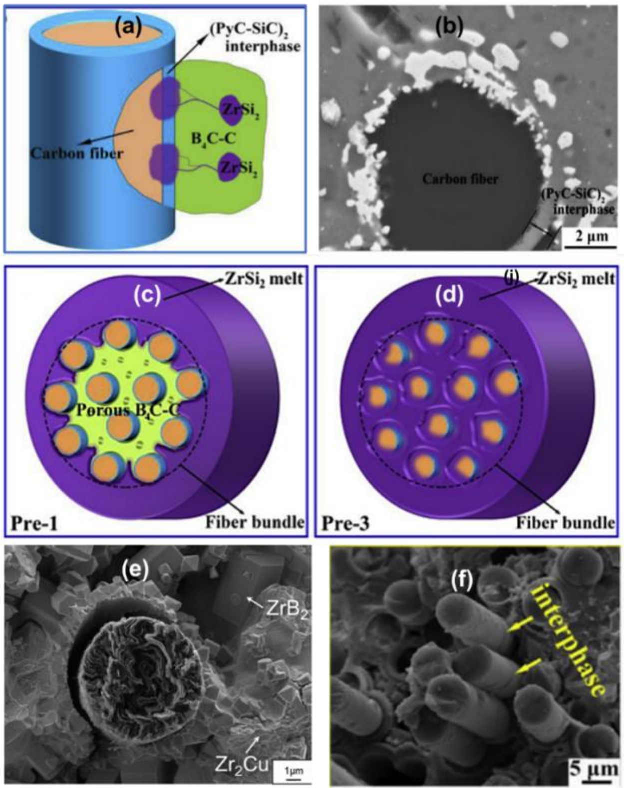

Figure 6: (a) Corrosion of carbon fibre and B_4C coating by $ZrSi_2$ melt during RMI[126]. (b) SEM image of the cross-section of a carbon fibre surrounded by a PyC coating and a SiC matrix[126]. (c)The effect of partially infiltrated fibre bundle and, (d) fully infiltrated fibre bundle[126]. (e)Fibre debonding from a ZrC-ZrB_2-Zr_2Cu matrix[106]. (f) Fibre pull-out from B_4C interphase coating and ZrC-SiC matrix after a bending test[126].

The typical stress-strain curve of a CMC-UHTC (Figure 7a) consists of an initially quasi-linear increase of strain with stress (region I), denoting pseudo-elastic behaviour. At a point in the linear relationship, the onset of cracking in the composite matrix is indicated by region II

(Figure 7a) in which the gradient of the linear relationship decreases. A kink or step in the linear relationship indicates crack deflection in the matrix or at the fibre/matrix interphase. The propagation of cracks weakens the composite, explaining the rapid strain at relatively low stress increases. At the peak of the curve (region III), the ultimate flexural strength is realised. Thereafter, the decrease in stress with increasing strain is observed, typically with pseudo-ductile fracture behaviour. Tests performed at 1500 °C revealed a sudden decrease of the stress due to the fractured composite showing significantly reduced resistance to failure in quasi-linear elastic region IV[130]. The ultimate failure occurs in region V. Gao *et al.*[131] also investigated how the flexural strength is affected by test temperature up to 1500 °C for a complex multiphase composite $MoSi_2(Cr_5Si_3)$–RSiC prepared from the RMI of $MoSi_2$−Si−Cr alloy into a SiC-based preform. Studies on the oxidation behaviour and ablation resistance of UHTCMCs composites in application-similar environments, and the subsequent mechanical performance changes, are important in determining the effects of the infiltration phases, preform characteristics and process parameters used in RMI. This subject is vast and deserves a separate review.

The desirable characteristics is for the CMC-UHTC composites to show a large range of pseudoplastic behaviour at high stresses by leveraging crack deflection, interfacial debonding, fibre bridging and fibre pull-out processes. These mechanisms delay composite failure and improve the flexural strength and fracture toughness of the composite. Figure 7b shows examples of carbon fibre-reinforced CMCs prepared by RMI with the melt phases introduced as immiscible metals, metallic alloys, including silicides, and metal element systems. The graph shows a general trend of higher infiltration temperatures resulting in lower flexural strengths in the composite produced. The work of Lee *et al.*[132] similarly showed how the flexural strength of the CMCs decreases with increasing RMI temperature in silicon carbide fibre-reinforced UHTC-CMCs prepared by RMI. On the other hand, Li *et al.*[133] showed that the bending strength of a C/ZrC-SiC composite without an interphase was 121 MPa, but with PyC and PyC/SiC interphases the bending strength improved by 83% and 149%, respectively, and the flexural modulus increased by 35% and 47%, respectively.

Galizia *et al.*[134] compared the mechanical performance of RMI-prepared UHTC-CMCs to processing methods as shown in Figure 7c. shows slurry-infiltration (SI) as a pre-RMI densification method using the same matrix phase. Although slurry infiltration, polymer infiltration and pyrolysis, chemical vapour infiltration and reactive gaseous infiltration are considered competing techniques to RMI, they can be utilised as pre-RMI densification processes. Thus, the advantages of RMI are better leveraged when combined with PIP[135], CVI[136], SI[134] and sol-gel[137]. Although PIP, CVI and room temperature SI processes do not damage fibres; PIP and SI produce relatively low-density composites than RMI[138]. On one hand, the PIP process involves complex and usually toxic precursors, and on the other hand, SI presents difficulties of fine particle sizes of the infiltrating materials to ensure mass transport into pores during filtration. As such, it is easier to use ceramics as precursors as they are easier to control fine particle sizes than metals. PIP, CVI, and SI are eligible densification processes because they can be performed repeatedly on the same composite until the required density is achieved. RMI cannot be repeated because of fibre damage and choking phenomena. The sol-gel process is still to be investigated further to validate its pros and cons.

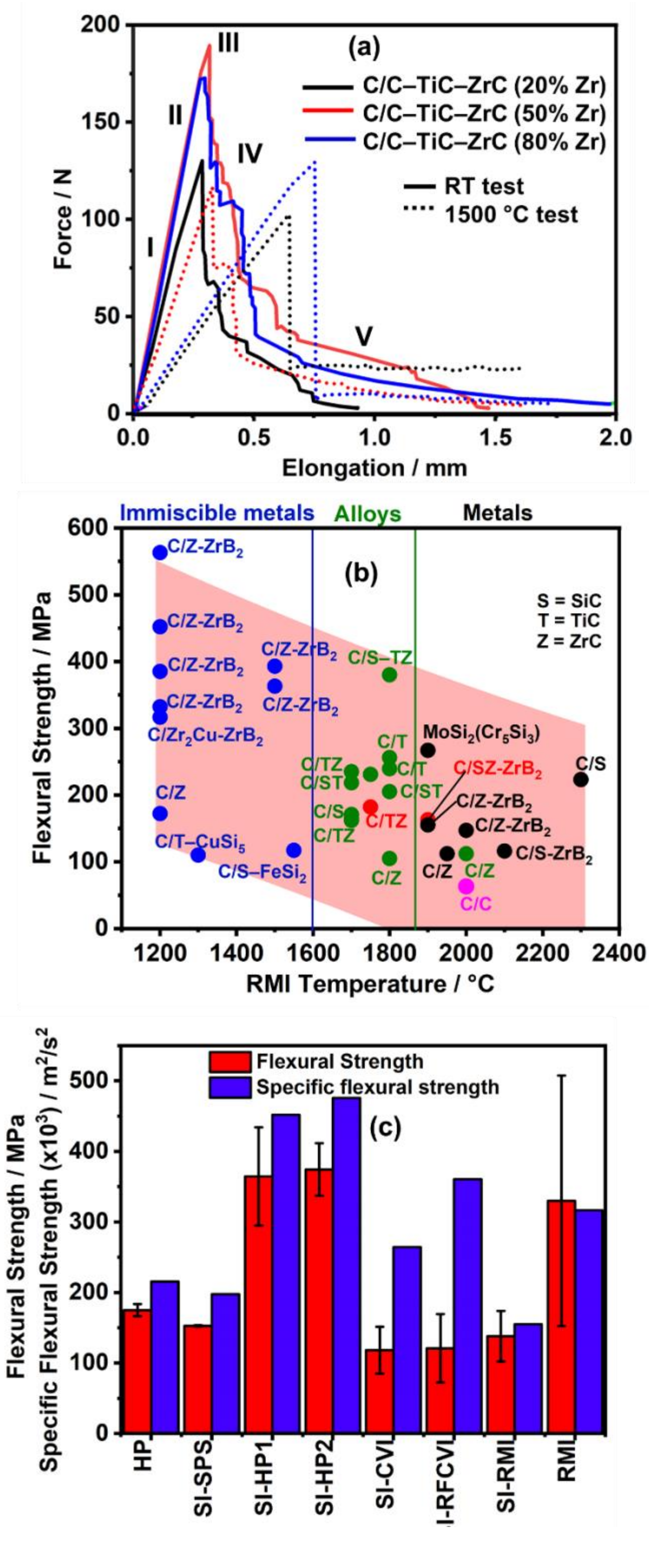

Figure 7: (e) Stress-strain curves of C/SiC-ZrC composite with varying amounts of Zr in the filtrating melt and tested at room temperature and 1500 °C[130]*. (b) Bending strength and flexural modulus of various UHTC-CMCs prepared by RMI* [30,39,65,74,100,106,126,131,134,136,139–147]*(c) Comparison of flexural strength and specific flexural strength graphs of UHTC composites prepared by other methods (HP=hot pressing, SI = silicon infiltration, SPS = spark plasma sintering, CVI = chemical vapour infiltration, RF = radio frequency, and RMI = reactive melt infiltration)*[134]*.*

5 Rapid Heating Techniques

Notwithstanding the high processing temperatures that the reactive melt infiltration process demands, rapid heating techniques such as spark plasma sintering (SPS), microwave assisted sintering (MAS)[148–150] and electromagnetic induction heating sintering (EIHS)[151,152] have been demonstrated for RMI processes. Such techniques are growing in application thanks to the short processing times they afford. Figure 8 shows schematically some rapid heating techniques for RMI. The European Union's HELM (High Frequency ElectroMagnetic technologies) project is using such approaches to improve RMI. Guo *et al.* [151] showed that electromagnetic induction heating reactive melt infiltration (EMIRMI) is achieved using heating rates of 300, 500 and 700 °C/min. At 700 °C/min, the heating rate was eighteen times faster than that using a conventional carbon tube furnace in the same investigation. On the other hand, the pulsed electric current sintering (field-assisted sintering technique/spark plasma sintering (FAST/SPS)) methods typically apply heating rates up to 250 °C/min. Microwave reactive infiltration of silicon into C/C and C/SiC composites showed heating rates of 360 °C/min at 2.45 GHz[148].

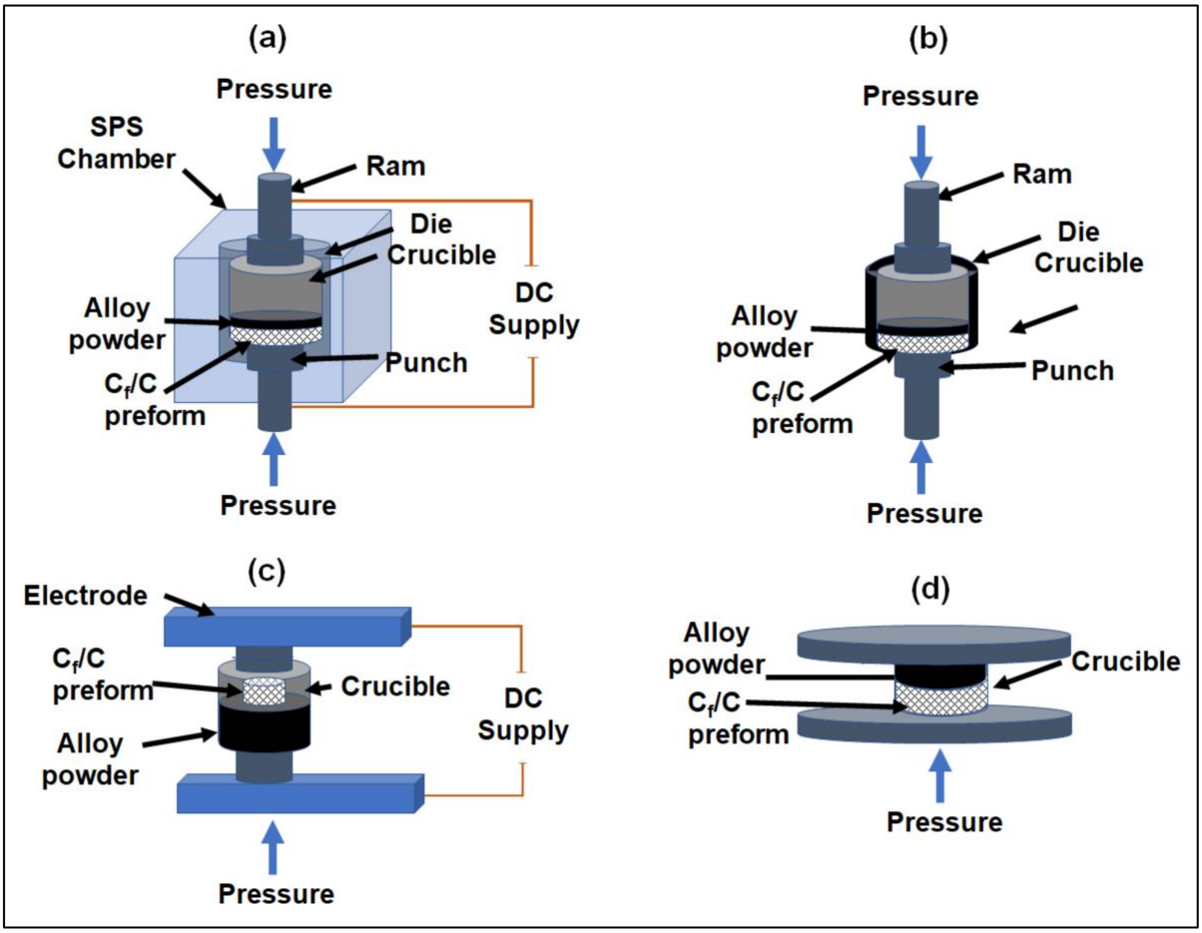

Figure 8: Schematic diagrams of fast-heating RMI arrangements (a) spark plasma sintering (b) high frequency induction heating[151,152] *(c) electrodes induction set-up*[153] *(d) carbon paper sandwich*[149,154]

6 Future Perspectives

Perfect net-shaping in complex geometry composites prepared by RMI is still a challenge. The application of additive manufacturing routes, particularly three-dimensional printing will be applied to realise homogeneous matrix microstructures. Additive manufacturing studies are already underway, for example, for ceramic composites[155–157] and for cermet composites[158,159]. Selective laser sintering[101,160,161] approaches have yet to be widely demonstrated for RMI preforms. The review by Koyanagi *et al.*[162] provides approaches for combining 3D-printing with RMI. The application of *in-situ* RMI and joining of the 3D-printed components to form larger parts on commercial scale is envisaged. Heidenreich[163] demonstrated *in situ* joining of a 5-part complex C/C-SiC using RMI.

The experience gathered from laboratory *in situ* RMI process monitoring will be scaled up to pilot plant and eventually industrial scale. Process control instrumentation will incorporate such elements to measure parameters such as infiltration height, infiltrated mass, and composite density. The use of process modelling covering mass transfer and heat and fluid flow as well as reaction kinetics, thermodynamics and microstructural evolution will be increasingly applied to RMI. Application of thermo-optical and spectroscopy techniques[120] for *in situ* analysis and thermal management in RMI is likely to expand. The integration of *in situ* visualisation of phase changes and mass transport will help monitor RMI progress. The testing and compilation of multiphase infiltrant properties pertinent to RMI is also likely to grow, for example, using high-temperature electrostatic levitator (HTESL) measurements as has been demonstrated at the Japan Space Utilization Promotion Centre[164]. Eventually, it is envisaged that these techniques will be applied commercially *in operandi* to give close quality control likely in sectors requiring this such as nuclear and defence.

High entropy alloys have yet to be integrated into composites via reactive melt infiltration, and this is an area ripe for exploration in the near future. If the concept of high entropy UHTCs is demonstrated to be commercially relevant, this will open a further extension of the RMI processing route.

7 Summary and Conclusions

Advanced multiphase ultra-high temperature ceramic composites have an important role in upgrading the oxidation resistance of C/SiC, SiC/SiC or SiC/C composites for aerospace and nuclear applications. Whether carbides, borides or nitrides are envisaged in the resultant ceramic matrix composite, RMI presents an optimization challenge of balancing the composition of the phases incorporated and the processing temperature to be used.

- Approaches for lowering the infiltration temperature are based on adjusting the constituent phases of the infiltrating material. Four approaches can be used to make multiphase UHTC systems of at least two transition metals and/or including Si, while circumventing high infiltration temperature challenges:
    a. Immiscible metallic systems involve RMI at temperature range 1100 to 1300 °C by utilizing molten copper as a carrier of the solid phase of the refractory metal of which the later forms the carbide UHTC. The Cu-Ti system is an exception to the immiscibility, however.
    b. Immiscible metallic systems combine at least two refractory metals to leverage their eutectic composition and temperature. This approach has been commonly used for M-Si and M_I-M_{II} alloys (M = refractory metal) as shown in
    c. Metal silicides systems have lower melting points than UHTCs, hence provide a low RMI temperature and double as sintering aids.
    d. Eutectic silicide systems involve combining at least two disilicides and/or penta-trisilicides to leverage their quasibinary eutectic point during RMI.

- Although RMI demands high processing temperatures, rapid heating techniques such as spark plasma sintering, microwave assisted sintering and electromagnetic induction heating sintering help to lower processing times. Heating rates of up to 700 °C/min have been demonstrated.
- Temperature gradients can occur in ceramic matrix composites during processing, leading to heterogeneous thermal spikes, thermal stresses and volume expansion changes. Temperature gradients of up to ~550 ℃ have been reported in silicon carbide composites.

- Homogeneous pore structures in the preform promote uniform infiltrant flow rates into the preform and uniform temperature profiles. This reduces microstructural defects (cracks, pores, uneven carbide grain growth, residual infiltrant matrix phases) in the resultant multiphase ceramic matrix composite.
- Applying barrier coatings protects the reinforcing fibres from corrosive effects of the infiltrating melt during RMI and improves the flexural strength and fracture toughness of the composite. Lower RMI temperatures and shorter processing times improve the fibres robustness for crack deflection, interfacial debonding, fibre bridging and fibre pull-out processes.
- Current efforts aim at preparing complex and homogeneous microstructure preforms prior to RMI. Integration of additive manufacturing and reactive melt infiltration into a single step is envisaged.
- Tracking thermophysical, thermochemical and thermomechanical properties in the composite during processing has been demonstrated by *in situ* laser-flash instrumentation and this will be applied more extensively in future, even *in operandi*.
- Increased use of process modelling including of mass transfer, heat and fluid flow, reaction kinetics, thermodynamics and microstructural evolution is envisaged, correlated with empirical data.

8 Acknowledgements

This work was funded through the Sêr Cymru II 80761-BU-103 project by Welsh European Funding Office (WEFO) under the European Development Fund (ERDF).

9 References

1. Fahrenholtz, W. G., Wuchina, E. J., Lee, W. E. & Zhou, Y. Introduction. in *Ultra-High Temperature Ceramics: Materials for Extreme Environment Applications* (ed. WG Fahrenholtz, EJ Wuchina, W. L. and Y. Z. (Editors)) 1–5 (Wiley, 2014).

2. Lee, W. E., Giorgi, E., Harrison, R., Maître, A. & Rapaud, O. Nuclear Applications for Ultra-High Temperature Ceramics and MAX Phases. in *Ultra-High Temperature Ceramics: Materials for Extreme Environment Applications* (ed. WG Fahrenholtz, EJ Wuchina, W. L. and Y. Z. (Editors)) 391–415 (Wiley, 2014).

3. Eric Wuchina, M. O. The Next Steps for Ultra-High Temperature Ceramics. in *Ultra-High Temperature Ceramics: Materials For Extreme Environmental Applications II, ECI Symposium Series* vol. 16 (2013).

4. Wuchina, E., Opila, E., Opeka, M., Fahrenholtz, W. & Talmy, I. UHTCs - Ultra-High Temperature Ceramic Materials for Extreme Environment Applications. *The Electrochemical Society Interface* **16**, 30–36 (2007).

5. Wang, Y., Zhu, X., Zhang, L. & Cheng, L. C/C-SiC-ZrC composites fabricated by reactive melt infiltration with Si 0.87Zr 0.13 alloy. *Ceramics International* **38**, 4337–4343 (2012).

6. Chen, Z. K., Xiong, X., Li, G. D. & Wang, Y. L. Ablation behaviors of carbon/carbon composites with C-SiC-TaC multi-interlayers. *Applied Surface Science* **255**, 9217–9223 (2009).

7. Zou, L., Wali, N., Yang, J. M., Bansal, N. P. & Yan, D. Microstructural characterization of a Cf/ZrC composite manufactured by reactive melt infiltration. *International Journal of Applied Ceramic Technology* **8**, 329–341 (2011).

8. Yi, W., Yongdong, X., Yiguang, W., Laifei, C. & Litong, Z. Effects of TaC addition on the ablation resistance of C/SiC. *Materials Letters* **64**, 2068–2071 (2010).

9. Qian, Y., Zhang, W., Ge, M. & Wei, X. Frictional response of a novel C/C-ZrB2-ZrC-SiC composite under simulated braking. *Journal of Advanced Ceramics* **2**, 157–161 (2013).

10. Li, J., Lenosky, T. J., Forst, C. J. & Yip, S. Thermochemical and Mechanical Stabilities of the Oxide Scale of ZrB2 + SiC and Oxygen Transport Mechanisms. *Journal of the American Ceramic Society* **1480**, 1475–1480 (2008).

11. Carney, C. M., Parthasarathy, T. A. & Cinibulk, M. K. Oxidation resistance of hafnium diboride ceramics with additions of silicon carbide and tungsten boride or tungsten carbide. *Journal of the American Ceramic Society* **94**, 2600–2607 (2011).

12. Wang, J., Hu, H., Zhang, Y., Wang, Q. & He, X. Preparation and characterization of C/SiC-ZrB2 composites via precursor infiltration and pyrolysis process. *Ceramic Transactions* **210**, 467–472 (2010).

13. Parthasarathy, T. A., Rapp, R. A., Opeka, M. & Kerans, R. J. A model for the oxidation of ZrB2, HfB2 and TiB2. *Acta Materialia* **55**, 5999–6010 (2007).

14. Monteverde, F., Bellosi, a. & Scatteia, L. Processing and properties of ultra-high temperature ceramics for space applications. *Materials Science and Engineering A* **485**, 415–421 (2008).

15. Bellosi, A., Monteverde, F. & Sciti, D. Fast densification of ultra-high-temperature ceramics by spark plasma sintering. *International Journal of Applied Ceramic Technology* **3**, 32–40 (2006).

16. Opeka, M. M., Talmy, I. G. & Zaykoski, J. A. Oxidation-based materials selection for 2000 °C+ hypersonic aerosurfaces: theoretical considerations and historical experience. *Journal of Materials Science* **39**, 5887–5904 (2004).

17. Eakins, E., Jayaseelan, D. D. & Lee, W. E. Toward oxidation-resistant ZrB2-SiC ultra high temperature ceramics. *Metallurgical and Materials Transactions A: Physical Metallurgy and Materials Science* **42**, 878–887 (2011).

18. Fahrenholtz, W. G. & Hilmas, G. E. Ultra-High Temperature Ceramics: Historic Perspectives and Recent Progress. *Ultra-High Temperature Ceramics: Materials For Extreme Environmental Applications II* (2012).

19. Derkewitz-Mattuck, J. B. *Kinetics of oxidation of refractory metals and alloys at 1000-2000 °C Part II, Technical Documentary Report NO. ASD-TDR-62-203*. (1963).

20. Kaufman, L. & Clougherty, E. *Investigation of boride compounds for very high temperature applications, Part I. No. TRD-TDR-63-4096-PT-1*. (1963).

21. Kaufman, L. & Clougherty, E. *Investigation of boride compounds for very high temperature applications, Part II. No. TRD-TDR-63-4096-PT-2.* (1965).

22. Steinitz, R., Binder, I. and Moskowitz, D. System molybdenum-boron and some properties of the molybdenum-borides. *JOM* **4**, 983–987 (1952).

23. Engelke, J. L., Halden, F. A. & Farley, E. P. *Synthesis of new high temperature materials, Technical report no. WADC 59- 654.* (1960).

24. MacDonald, N. F., and C. E. R. The oxidation of hot-pressed titanium carbide and titanium boride in the temperature range 300°–1000° C. *Powder Metallurgy* **2**, 172–176 (1959).

25. Voitovich, R. F. & Pugach, E. A. High-temperature oxidation characteristics of the carbides of the group VI transition metals. *Institute of Materials Science, Academy of Sciences of the Ukrainian SSR.Translated from Porosh- kovaya Metallurgiya, No. 4 (124), pp. 59-64, April, 1973.* **21**, 1154–1157 (1973).

26. Harrison, R. W. & Lee, W. E. Mechanism and Kinetics of Oxidation of ZrN Ceramics. *Journal of the American Ceramic Society* **98**, 2205–2213 (2015).

27. Harrison, R. W. & Lee, W. E. Processing and properties of ZrC, ZrN and ZrCN ceramics: a review. *Advances in Applied Ceramics* **115**, 294–307 (2016).

28. Wang, D., Chen, H., Wang, Y. & Wei, B. Precipitations of W/Cu metallic phases in ZrC in the reactive melt in fi ltrated ZrC/W composite. *Journal of Alloys and Compounds* **843**, 155919 (2020).

29. Khoee, A. A., Habibolahzadeh, A., Qods, F. & Baharvandi, H. Study on rheological behavior of WC slurry in gel-casting process and reactive infiltration of produced foam by molten Zr2Cu alloy. *International Journal of Refractory Metals and Hard Materials* **46**, 30–34 (2014).

30. Camarano, A., Caccia, M., Molina, J. M. & Narciso, J. Effects of Fe addition on the mechanical and thermo-mechanical properties of SiC/FeSi2/Si composites produced via reactive infiltration. *Ceramics International* **42**, 10726–10733 (2016).

31. Peng, J., Lara-curzio, E. & Shin, D. Calphad High-throughput thermodynamic screening of carbide / refractory metal cermets for ultra-high temperature applications ☆. *Calphad* **66**, 101631 (2019).

32. Liu, J. L. *et al.* Experimental investigation on phase equilibria of Cu–Ti–Hf system and performance of Cu(Ti, Hf)2 phase. *Journal of Materials Science* **53**, 7809–7821 (2018).

33. Wang, D. & Wang, Y. Mechanism of Incongruent Reactions Between Zr-Cu Melts and Solid Tungsten Carbide. *Metallurgical and Materials Transactions B: Process Metallurgy and Materials Processing Science* **51**, 1603–1616 (2020).

34. Massalski, T. B., Okamoto, H., Subramanian, P. R. & Kacprzak, L. *Binary Alloy Phase Diagrams*. (Wiliam W. Scott Pub., 1990).

35. Turchanin, M. A., Agraval, P. G. & Abdulov, A. R. Thermodynamic assessment of the Cu-Ti-Zr system I. Cu-Ti system. *Powder Metallurgy and Metal Ceramics* **47**, 344–360 (2008).

36. Valenza, F., Gambaro, S., Muolo, M. L., Salvo, M. & Casalegno, V. Wetting of SiC by Al-Ti alloys and joining by in-situ formation of interfacial Ti3Si(Al)C2. *J Eur Ceram Soc* **38**, 3727–3734 (2018).

37. Laurila, T., Zeng, K., Kivilahti, J. K., Molarius, J. & Suni, I. Amorphous layer formation at the TaC/Cu interface in the Si/TaC/Cu metallization system. *Applied Physics Letters* **80**, 938–940 (2002).

38. Zeng, Y. *et al.* Microstructure and ablation behavior of carbon/carbon composites infiltrated with Zr-Ti. *Carbon N Y* **54**, 300–309 (2013).

39. Arai, Y., Marumo, T. & Inoue, R. Use of zr–ti alloy melt infiltration for fabricating carbon-fiber-reinforced ultrahigh-temperature ceramic matrix composites. *Journal of Composites Science* **5**, (2021).

40. Roger, J. & Salles, M. Kinetics of liquid metal infiltration in TiC-SiC or SiC porous compacts. *Journal of Alloys and Compounds* **860**, 158453 (2021).

41. Roger, J. & Salles, M. Thermodynamic of liquid metal in fi ltration in TiC-SiC or SiC porous compacts. *Journal of Alloys and Compounds* **802**, 636–648 (2019).

42. Krenkel, W. & Schanz, P. Fiber ceramic structures based on liquid impregnation technique. *Acta Astronautica* **28**, 159–169 (1992).

43. Singh, M. & Behrendt, D. R. Reactive melt infiltration of silicon-niobium alloys in microporous carbons. *Journal of Materials Research* **9**, 1701–1708 (1994).

44. Nesmelov, D. D., Ordan'yan, S. S. & Udalov, Y. P. Structure and Mechanical Properties of Hot-Pressed Composite Ceramics W2B5–ZrB2–SiC–B4C. *Refractories and Industrial Ceramics* **62**, 202–207 (2021).

45. Tu, R. *et al.* Mechanical, electrical and thermal properties of ZrC-ZrB2-SiC ternary eutectic composites prepared by arc melting. *J Eur Ceram Soc* **38**, 3759–3766 (2018).

46. Makurunje, P., Monteverde, F. & Sigalas, I. Self-generating oxidation protective high-temperature glass-ceramic coatings for Cf/C-SiC-TiC-TaC UHTC matrix composites. *J Eur Ceram Soc* **37**, 3227–3239 (2017).

47. Shah, D. M. MoSi2 and other silicides as high temperature structural materials. *Superalloys* 409–422 (1992).

48. Wei, F. G., Kimura, Y. & Mishima, Y. Microstructure and phase stability in MoSi2-TSi2 (T=Cr, V, Nb, Ta, Ti) pseudo-binary systems. *Materials Transactions* vol. 42 1349–1355 Preprint at https://doi.org/10.2320/matertrans.42.1349 (2001).

49. Silvestroni, L., Guicciardi, S., Nygren, M., Melandri, C. & Sciti, D. Effect of the sintering additive on microstructure and mechanical properties of Hi-nicalon^{TM} SiC fibers in a HfB2 matrix. *Journal of the American Ceramic Society* **96**, 643–650 (2013).

50. Sciti, D., Silvestroni, L., Celotti, G., Melandri, C. & Guicciardi, S. Sintering and Mechanical Properties of ZrB2-TaSi2 and HfB2-TaSi2 Ceramic Composites. *Journal of the American Ceramic Society* **91**, 3285–3291 (2008).

51. Sciti, D., Silvestroni, L. & Nygren, M. Spark plasma sintering of Zr- and Hf-borides with decreasing amounts of MoSi2 as sintering aid. *J Eur Ceram Soc* **28**, 1287–1296 (2008).

52. Ren, X. *et al.* Influence of MoSi2 on oxidation protective ability of TaB2-SiC coating in oxygen-containing environments within a broad temperature range. *Journal of Advanced Ceramics* **9**, 703–715 (2020).

53. Sciti, D., Silvestroni, L., Saccone, G. & Alfano, D. Effect of different sintering aids on thermo-mechanical properties and oxidation of SiC fibers - Reinforced ZrB2 composites. *Materials Chemistry and Physics* **137**, 834–842 (2013).

54. Silvestroni, L. & Sciti, D. Effect of transition metal silicides on microstructure and mechanical properties of ultra-high temperature ceramics. *MAX Phases and Ultra-High Temperature Ceramics for Extreme Environments* (2013) doi:10.4018/978-1-4666-4066-5.ch005.

55. Silvestroni, L. & Sciti, D. Densification of ZrB2-TaSi2 and HfB2-TaSi2 Ultra-High-Temperature Ceramic Composites. *Journal of the American Ceramic Society* **94**, 1920–1930 (2011).

56. Silvestroni, L., Sciti, D., Kling, J., Lauterbach, S. & Kleebe, H. J. Sintering mechanisms of zirconium and hafnium carbides doped with MoSi 2. *Journal of the American Ceramic Society* **92**, 1574–1579 (2009).

57. Telle, R. The quasi ternary system TiB2-CrB2-WB2 between 1500 and 1900°C and the related quasi binary subsystems. *J Eur Ceram Soc* **39**, 3677–3683 (2019).

58. Kumar, K. C. H., Wollants, P. & Delacy, L. Thermodynamic assessment of the Ti-Zr system and calculation of the Nb-Ti-Zr phase diagram. *J. Alloys Compd.* **206**, 121–127 (1994).

59. Meier, S. & Heinrich, J. G. Processing-microstructure-properties relationships of MoSi2-SiC composites. *J Eur Ceram Soc* **22**, 2357–2363 (2002).

60. Makurunje, P., Sigalas, I. & Binner, J. Scale characterisation of an oxidised (Hf,Ti)C-SiC ultra-high temperature ceramic matrix composite. *J Eur Ceram Soc* **41**, 167–175 (2021).

61. Makurunje, P. S. Fabrication of a C/C-SiC-TiC-TaC composite by hybrid wet infiltration. (University of the Witwatersrand, Johannesburg, 2015).

62. Makurunje, P., Sigalas, I. & Binner, J. Surface oxidation and thermochemical stability of a Cf/WC hybrid-UHTC composite. *Unpublished*.

63. Gnesin, I. B. & Gnesin, B. A. Structure and properties of a silicide-carbide protective coating on carbon-carbon composites. *Metal Science and Heat Treatment* **62**, 393–398 (2020).

64. Maksimov V.A., and S. F. I. Phase diagram of the W-Ti-Si system. *Russ. Metall.* 129–133 (1970).

65. Wu, H., Yi, M., Ge, Y., Peng, K. & Ran, L. Microstructural development of a C/C-ZrC-Cu composite prepared by reactive melt infiltration with Zr/Cu powder mixture. *Materials Characterization* **138**, 238–244 (2018).

66. Wang, D., Wang, Y., Deng, W., Song, G. & Zhou, Y. Microstructure and mechanical properties of Mo-ZrC-Cu composites synthesized by reactive melt infiltration of Zr-Cu melt into porous Mo2C preforms at 1300 °C. *Materials Chemistry and Physics* **212**, 51–59 (2018).

67. Wang, D., Chen, H., Wang, Y. & Wei, B. Precipitations of W/Cu metallic phases in ZrC in the reactive melt infiltrated ZrC/W composite. *Journal of Alloys and Compounds* **843**, 155919 (2020).

68. Wang, D. *et al.* W-ZrC composites prepared by reactive melt infiltration of Zr2Cu alloy into partially carburized W preforms. *International Journal of Refractory Metals and Hard Materials* **67**, 125–128 (2017).

69. Zhao, Y. W., Wang, Y. J., Peng, H. X. & Zhou, Y. Dense sub-micron-sized ZrC-W composite produced by reactive melt infiltration at 1200 °c. *International Journal of Refractory Metals and Hard Materials* **30**, 196–199 (2012).

70. Wang, D. *et al.* Effect of W content on the ablation properties of W-ZrC composites synthesized by reactive melt infiltration under oxyacetylene flame. *International Journal of Refractory Metals and Hard Materials* **74**, 28–39 (2018).

71. Zhang, K. X., Guo, X. S., Zhao, W. K., Zhang, F. Q. & He, L. L. TEM study on the microstructure of the interface at the scale of nanometer formed between Cu-8 wt.% Ti melt and C/C preform. *Materials Chemistry and Physics* **246**, (2020).

72. Wang, D., Wei, B., Wang, Y., Song, G. & Zhou, Y. Microstructure and mechanical properties of intragranular W-Cu/TiC-ZrC composite prepared by reactive melt infiltration at 1300 °C. *Materials Characterization* **138**, 89–97 (2018).

73. Rambo, C. R., Travitzky, N., Zimmermann, K. & Greil, P. Synthesis of TiC/Ti-Cu composites by pressureless reactive infiltration of TiCu alloy into carbon preforms fabricated by 3D-printing. *Materials Letters* **59**, 1028–1031 (2005).

74. Xiao, P. *et al.* Microstructure and properties of Cu-Ti alloy infiltrated chopped Cf reinforced ceramics composites. *Ceramics International* **43**, 16628–16637 (2017).

75. Kudielka, H. & Nowotny, H. Si-Ta-Ti Phase Diagram. *ASM Alloy Phase Diagrams Centre* http://www.asminternational.org/asmenterprise/APD (1956).

76. Dokukina, N. V. & ShamraI, F. I. Phase equilibrium in the system W-Nb-Si and certain properties of alloys. *Translated from Poroshkovaya Metallurgiya* **6**, 427–435 (1962).

77. Rokhlin, L. Molybdenum - Silicon - Tantalum. in *Refractory metal systems, Landolt-Börnstein - Group IV Physical Chemistry, Volume 11E3.* 385 (Springer-Verlag Berlin Heidelberg, 2010).

78. Chen, X. *et al.* Ablation behavior of three-dimensional Cf/SiC-ZrC-ZrB2 composites prepared by a joint process of sol-gel and reactive melt infiltration. *Corrosion Science* **134**, 49–56 (2018).

79. Chen, X. *et al.* Microstructure and mechanical properties of three dimensional Cf/SiC-ZrC-ZrB2composites prepared by reactive melt infiltration method. *J Eur Ceram Soc* **36**, 3969–3976 (2016).

80. Chen, X., Feng, Q., Kan, Y., Ni, D., Zhou, H., Gao, L., Zhang, X., Ding, Y. and Dong, S. Effects of preform pore structure on infiltration kinetics and microstructure evolution of RMI-derived Cf/ZrC-ZrB2-SiC composite. *J Eur Ceram Soc* **40**, 2683-2690. (2020).

81. Xue, C. *et al.* Fabrication and microstructure of ZrB2–ZrC–SiC coatings on C/C composites by reactive melt infiltration using ZrSi2 alloy. *Journal of Advanced Ceramics* **7**, 64–71 (2018).

82. Xin, Y. *et al.* Ablative property and mechanism of C/C-ZrB2-ZrC-SiC composites reinforced by SiC networks under plasma flame. *Corrosion Science* **107**, 9–20 (2016).

83. Tatarko, P. *et al.* Design of Lu2O3-reinforced Cf/SiC-ZrB2-ZrC ultra-high temperature ceramic matrix composites: Wetting and interfacial reactivity by ZrSi2 based alloys. *J Eur Ceram Soc* **41**, 1–10 (2020).

84. Zeng, Y. *et al.* Ablation-resistant carbide Zr0.8Ti0.2C0.74B0.26for oxidizing environments up to 3,000 °c. *Nature Communications* **8**, 1–9 (2017).

85. Hao, Z., Sun, W., Xiong, X., Chen, Z. & Wang, Y. Effects of Ti/Al addition on the microstructures and ablation properties of Cf/C-MoSi2-SiC composites. *J Eur Ceram Soc* **36**, 457–464 (2016).

86. Sribalaji, M., Mukherjee, B., Islam, A. & Kumar Keshri, A. Microstructural and mechanical behavior of spark plasma sintered titanium carbide with hybrid reinforcement of tungsten carbide and carbon nanotubes. *Materials Science and Engineering A* **702**, 10–21 (2017).

87. Esfehanian, M., Günster, J., Moztarzadeh, F. & Heinrich, J. G. Development of a high temperature Cf/XSi2-SiC (X = Mo, Ti) composite via reactive melt infiltration. *J Eur Ceram Soc* **27**, 1229–1235 (2007).

88. Hucke, E. E. *Process Development for Silicon Carbide Based Structural Ceramics, AMMRC TR 81-13*. (1981).

89. Bai, S., Ye, Y., Tong, Y. & Zhang, H. Reactive melt infiltration of carbon fiber reinforced ceramic composites. in *Low, I. M. (Ed.). (2013). MAX phases and ultra-high temperature ceramics for extreme environments*. 323–347 (IGI Global., 2013).

90. Sangsuwan, P., Tewari, S. N., Gatica, J. E., Singh, M. & Dickerson, R. Reactive infiltration of silicon melt through microporous amorphous carbon preforms. *Metallurgical and Materials Transactions B: Process Metallurgy and Materials Processing Science* **30**, 933–944 (1999).

91. Calderon, N. R., Martínez-Escandell, M., Narciso, J. & Rodríguez-Reinoso, F. The combined effect of porosity and reactivity of the carbon preforms on the properties of

SiC produced by reactive infiltration with liquid Si. *Carbon N Y* **47**, 2200–2210 (2009).

92. Schulte-Fischedick, J. *et al.* The morphology of silicon carbide in C/C-SiC composites. *Materials Science and Engineering A* **332**, 146–152 (2002).

93. Roger, J. & Chollon, G. Mechanisms and kinetics during reactive infiltration of molten silicon in porous graphite. *Ceramics International* **45**, 8690–8699 (2019).

94. Wang, Y., Zhu, X., Zhang, L. & Cheng, L. Reaction kinetics and ablation properties of C/C-ZrC composites fabricated by reactive melt infiltration. *Ceramics International* **37**, 1277–1283 (2011).

95. Suyama, S., Itoh, Y., Kohyama, A. & Katoh, Y. Effect of residual silicon phase on reaction-sintered silicon carbide. in *Advanced SiC/SiC Ceramic Composites: Developments and Applications in Energy Systems, 144* 181–188 (2012).

96. Kütemeyer, M., Schomer, L., Helmreich, T., Rosiwal, S. & Koch, D. Fabrication of ultra high temperature ceramic matrix composites using a reactive melt infiltration process. *J Eur Ceram Soc* **36**, 3647–3655 (2016).

97. Caccia, M. & Narciso, J. On the effects of hot spot formation during MW-assisted synthesis of Cf/SiC composites by reactive melt infiltration: Experimental simulations through high temperature treatments. *J Eur Ceram Soc* **40**, 28–35 (2020).

98. Hase, T. & Suzuki, H. Rise in temperature of SiC pellet involving reaction sintering. *Bulletin of the Research Laboratory for Nuclear Reactors Tokyo Institute of Technology.* **1**, 37–42 (1976).

99. Hucke, E. E. *Process Development for Silicon Carbide Based Structural Ceramics, AMMRC TR 83-5*. (1983).

100. Pi, H., Fan, S. & Wang, Y. C/SiC-ZrB2-ZrC composites fabricated by reactive melt infiltration with ZrSi2 alloy. *Ceramics International* **38**, 6541–6548 (2012).

101. Zhong, Q. *et al.* Reactive melt infiltrated Cf/SiC composites with robust matrix derived from novel engineered pyrolytic carbon structure. *Ceramics International* **43**, 5832–5836 (2017).

102. Ye, Y., Zhang, H., Tong, Y. & Bai, S. HfC-based coating prepared by reactive melt infiltration on C/C composite substrate. *Ceramics International* **39**, 5477–5483 (2013).

103. Guo, W., Ye, Y., Bai, S., Zhu, L. & Li, S. Preparation and formation mechanism of C/C–SiC composites using polymer-Si slurry reactive melt infiltration. *Ceramics International* **46**, 5586–5593 (2020).

104. Zhou, Z. *et al.* Microstructure and ablation performance of SiC–ZrC coated C/C composites prepared by reactive melt infiltration. *Ceramics International* **44**, 8314–8321 (2018).

105. Chang, Y. *et al.* Microstructure and ablation behaviors of a novel gradient C/C-ZrC-SiC composite fabricated by an improved reactive melt infiltration. *Ceramics International* **42**, 16906–16915 (2016).

106. Vinci, A. *et al.* Reactive melt infiltration of carbon fibre reinforced ZrB2/B composites with Zr2Cu. *Composites Part A: Applied Science and Manufacturing* **137**, (2020).

107. Erdely, P. *et al.* In situ characterization techniques based on synchrotron radiation and neutrons applied for the development of an engineering intermetallic titanium aluminide alloy. *Metals (Basel)* **6**, 1–27 (2016).

108. Liu, J. *et al.* In situ infiltration behavior and interfacial microstructure evolution between Al and carbon fibers. *Journal of Alloys and Compounds* **853**, 157120 (2021).

109. Watson, I. J. *et al.* In situ characterization of a Nb and Mo containing γ-TiAl based alloy using neutron diffraction and high-temperature microscopy. *Advanced Engineering Materials* **11**, 932–937 (2009).

110. Larson, N. M. & Zok, F. W. In-situ 3D visualization of composite microstructure during polymer-to-ceramic conversion. *Acta Materialia* **144**, 579–589 (2018).

111. Bale, H. A. *et al.* Real-time quantitative imaging of failure events in materials under load at temperatures above 1,600 °C. *Nat Mater* **12**, 40–6 (2013).

112. Haboub, A. *et al.* Tensile testing of materials at high temperatures above 1700 degrees C with in situ synchrotron X-ray micro-tomography. *Review of Scientific Instruments* **85**, 1–13 (2014).

113. Roger, J. *et al.* SiC / Si composites elaboration by capillary infiltration of molten silicon To cite this version : HAL Id : hal-01728175. (2018).

114. Naikade, M. *et al.* Liquid metal infiltration of silicon based alloys into porous carbonaceous materials. Part II: Experimental verification of modelling approaches by infiltration of Si-Zr alloy into idealized microchannels. *J Eur Ceram Soc* **42**, 1984–1994 (2022).

115. Calderon, N. R., Voytovych, R., Narciso, J. & Eustathopoulos, N. Wetting dynamics versus interfacial reactivity of AlSi alloys on carbon. *Journal of Materials Science* **45**, 2150–2156 (2010).

116. Voytovych, R., Israel, R., Calderon, N., Hodaj, F. & Eustathopoulos, N. Reactivity between liquid Si or Si alloys and graphite. *J Eur Ceram Soc* **32**, 3825–3835 (2012).

117. Protsenko, P., Garandet, J. P., Voytovych, R. & Eustathopoulos, N. Thermodynamics and kinetics of dissolutive wetting of Si by liquid Cu. *Acta Materialia* **58**, 6565–6574 (2010).

118. Caccia, M. *et al.* Towards optimization of SiC/CoSi2 composite material manufacture via reactive infiltration: Wetting study of Si-Co alloys on carbon materials. *J Eur Ceram Soc* **35**, 4099–4106 (2015).

119. Giuranno, D., Polkowski, W., Bruzda, G., Kudyba, A. & Narciso, J. Interfacial phenomena between liquid Si-rich Si-Zr alloys and glassy carbon. *Materials* **13**, 1–15 (2020).

120. Raether, F., Baber, J. and Friedrich, H. Thermal Management of Heating Processes– Measuring Heat Transfer Properties. *Refractories Worldforum* **11**, 59–65 (2019).

121. Hofbauer, P. J., Rädlein, E. & Raether, F. Fundamental Mechanisms With Reactive Infiltration of Silicon Melt Into Carbon Capillaries. *Advanced Engineering Materials* **1900184**, 1–11 (2019).

122. Mainzer, B., Kelm, K., Watermeyer, P., Frieß, M. & Koch, D. How to tame the aggressiveness of liquid silicon in the LSI process. *Key Engineering Materials* **742 KEM**, 238–245 (2017).

123. Tsunoura, T., Yoshida, K., Yano, T., Aoki, T. & Ogasawara, T. Fabrication and bending behavior of amorphous SiC-fiber-reinforced Si-Co eutectic alloy composites at elevated temperatures. *Composites Part B: Engineering* **164**, 769–777 (2019).

124. Tong, Y., Bai, S., Zhang, H. & Chen, K. C/C-SiC composite prepared by Si-10Zr alloyed melt infiltration. *Ceramics International* **38**, 3301–3307 (2012).

125. Makurunje, P., Dziike, F. & Sigalas, I. Multiphase ultra-high temperature ceramic barrier coatings on fibers in extreme environments. in *Ceramic Science and Engineering: Basics to Recent Advancements* (eds. Misra, K. P. & Misra, R. D. K.) 525–542 (Elsevier, 2022).

126. Chen, X., Ni, D., Kan, Y., Jiang, Y., Zhou, H., Wang, Z. and D. Reaction mechanism and microstructure development of ZrSi2 melt-infiltrated Cf/SiC-ZrC-ZrB2 composites: The influence of preform pore structures. *Journal of Materiomics* **4**, 266–275 (2018).

127. Kütemeyer M, Shandler D, Koch D, F. M. Reactive Melt Infiltration of Boron Containing Fiber Reinforced Preforms Forming a ZrB2 Matrix. in *Prop. Adv. Ceram. Compos. VII* 169–80 (John Wiley & Sons, Ltd, 2015).

128. Aoki, T., Ogasawara, T., Okubo, Y., Yoshida, K. & Yano, T. Fabrication and properties of Si-Hf alloy melt-infiltrated Tyranno ZMI fiber/SiC-based matrix composites. *Composites Part A: Applied Science and Manufacturing* **66**, 155–162 (2014).

129. Shim, G. *et al.* Influence of pyrolysis and melt infiltration temperatures on the mechanical properties of SiCf/SiC composites. *Ceramics International* **48**, 1532–1541 (2022).

130. Marumo, T. *et al.* Characterization of carbon fiber-reinforced ultra-high temperature ceramic matrix composites fabricated via Zr-Ti alloy melt infiltration. *J Eur Ceram Soc* **42**, 5208–5219 (2022).

131. Gao, P. zhao, Cheng, L., Yuan, Z., Liu, X. pan & Xiao, H. ning. High temperature mechanical retention characteristics and oxidation behaviors of the MoSi2(Cr5Si3)—RSiC composites prepared via a PIP—AAMI combined process. *Journal of Advanced Ceramics* **8**, 196–208 (2019).

132. Lee, S. P. *et al.* High temperature characterization of reaction sintered SiC based materials. *Journal of Nuclear Materials* **329–333**, 534–538 (2004).

133. Li, Q., Dong, S., Wang, Z. & Shi, G. Fabrication and properties of 3-D Cf/ZrC-SiC composites by the vapor silicon infiltration process. *Ceramics International* **39**, 4723–4727 (2013).

134. Galizia, P. *et al.* Retained strength of UHTCMCs after oxidation at 2278 K. *Composites Part A: Applied Science and Manufacturing* **149**, 106523 (2021).

135. Guo, W., Ye, Y., Bai, S., Zhu, L. & Li, S. Preparation and formation mechanism of C/C–SiC composites using polymer-Si slurry reactive melt infiltration. *Ceramics International* **46**, 5586–5593 (2020).

136. Tong, Y., Bai, S. & Chen, K. C/C-ZrC composite prepared by chemical vapor infiltration combined with alloyed reactive melt infiltration. *Ceramics International* **38**, 5723–5730 (2012).

137. Chen, X. *et al.* 3D Cf/SiC-ZrC-ZrB2 composites fabricated via sol-gel process combined with reactive melt infiltration. *J Eur Ceram Soc* **36**, 3607–3613 (2016).

138. Zhao, D., Zhang, C., Hu, H. & Zhang, Y. Preparation and characterization of three-dimensional carbon fiber reinforced zirconium carbide composite by precursor infiltration and pyrolysis process. *Ceramics International* **37**, 2089–2093 (2011).

139. Ni, Y., Luo, R. & Luo, H. Fabrication and mechanical properties of 3-D Cf/C-SiC-TiC composites prepared by RMI. *Journal of Alloys and Compounds* **798**, 784–789 (2019).

140. Wang. C.C-SiC-ZrC Composites Fabricated by Reactive Melt Infiltration with Si0.87Zr0.13 alloy.

141. Ni, Y. & Luo, R. Microstructure and mechanical properties of carbon/carbon composites infiltrated with ti–6al–4v titanium alloy. *Crystals (Basel)* **10**, (2020).

142. Kütemeyer, M., Helmreich, T., Rosiwal, S. & Koch, D. Influence of zirconium-based alloys on manufacturing and mechanical properties of ultra high temperature ceramic matrix composites. *Advances in Applied Ceramics* **117**, s62–s69 (2018).

143. Chen, S., Li, G., Hu, H., Li, Y. & Mei, M. Microstructure and properties of ablative C/ZrC–SiC composites prepared by reactive melt infiltration of zirconium and vapour silicon infiltration. *Ceramics International* **43**, 3439–3442 (2017).

144. Chen, S., Zhang, C., Zhang, Y. & Hu, H. Preparation and properties of carbon fiber reinforced ZrC-ZrB2 based composites via reactive melt infiltration. *Composites Part B: Engineering* **60**, 222–226 (2014).

145. Zhu, Y. *et al.* Microstructure and mechanical properties of Cf/ZrC composites fabricated by reactive melt infiltration at relatively low temperature. *Ceramics International* **39**, 9085–9089 (2013).

146. Zhang, S., Wang, S., Li, W., Zhu, Y. & Chen, Z. Preparation of ZrB2 based composites by reactive melt infiltration at relative low temperature. *Materials Letters* **65**, 2910–2912 (2011).

147. Liu, Y., Fu, Q., Wang, B., Liu, T. & Sun, J. The ablation behavior and mechanical property of C/C-SiC-ZrB2 composites fabricated by reactive melt infiltration. *Ceramics International* **43**, 6138–6147 (2017).

148. Bianchi, G. *et al.* Reactive silicon infiltration of carbon bonded preforms embedded in powder field modifiers heated by microwaves. *Ceramics International* **41**, 12439–12446 (2015).

149. Padovano, E. *et al.* Graphite-Si-SiC ceramics produced by microwave assisted reactive melt infiltration. *J Eur Ceram Soc* **39**, 2232–2243 (2019).

150. Cornolti, L., Martinelli, S., Bianchi, G. & Ortona, A. Microwave heating controlled reactive melt infiltration for graphite-Si-SiC ceramics manufacturing. *Journal of the American Ceramic Society* **102**, 2304–2315 (2019).

151. Guo, W., Bai, S. & Ye, Y. Controllable fabrication and mechanical properties of C/C–SiC composites based on an electromagnetic induction heating reactive melt infiltration. *J Eur Ceram Soc* **41**, 2347–2355 (2021).

152. Kwon, S. M., Lee, S. J. & Shon, I. J. Enhanced properties of nanostructured ZrO2-graphene composites rapidly sintered via high-frequency induction heating. *Ceramics International* **41**, 835–842 (2015).

153. Mukasyan, A. S. & White, J. D. E. Electrically induced liquid infiltration for the synthesis of carbon/carbon-silicon carbide composite. *Ceramics International* **35**, 3291–3299 (2009).

154. Wang, C. *et al.* A general method to synthesize and sinter bulk ceramics in seconds. *Science (1979)* **368**, 521–526 (2020).

155. Wahl, L., Lorenz, M., Biggemann, J. & Travitzky, N. Robocasting of reaction bonded silicon carbide structures. *J Eur Ceram Soc* **39**, 4520–4526 (2019).

156. Zhang, H., Yang, Y., Liu, B. & Huang, Z. The preparation of SiC-based ceramics by one novel strategy combined 3D printing technology and liquid silicon in fi ltration process. *Ceramics International* **45**, 10800–10804 (2019).

157. Moon, J., Caballero, A. C., Hozer, L., Chiang, Y. M. & Cima, M. J. Fabrication of functionally graded reaction infiltrated SiC-Si composite by three-dimensional printing (3DP^{TM}) process. *Materials Science and Engineering A* **298**, 110–119 (2001).

158. Cramer, C. L., Wieber, N. R., Aguirre, T. G., Lowden, R. A. & Elliott, A. M. Shape retention and infiltration height in complex WC-Co parts made via binder jet of WC with subsequent Co melt infiltration. *Additive Manufacturing* **29**, 100828 (2019).

159. Cramer, C. L., Nandwana, P., Lowden, R. A. & Elliott, A. M. Infiltration studies of additive manufacture of WC with Co using binder jetting and pressureless melt method. *Additive Manufacturing* **28**, 333–343 (2019).

160. Xiong, H. *et al.* Composites : Part B Effects of binders on dimensional accuracy and mechanical properties of SiC particulates preforms fabricated by selective laser sintering. *Composites Part B* **44**, 480–483 (2013).

161. Jin, L., Zhang, K., Xu, T., Zeng, T. & Cheng, S. The fabrication and mechanical properties of SiC / SiC composites prepared by SLS combined with PIP. *Ceramics International* **44**, 20992–20999 (2018).

162. Koyanagi, T., Terrani, K., Harrison, S., Liu, J. & Katoh, Y. Additive manufacturing of silicon carbide for nuclear applications. *Journal of Nuclear Materials* **543**, 152577 (2021).

163. Heidenreich, B. Melt infiltration process. in *Ceramic Matrix Composites: Fiber Reinforced Ceramics and Their Applications* (ed. W Krenkel.) 113–139 (2008).

164. Rhim, W. & Ohsaka, K. Thermophysical properties measurement of molten silicon by high-temperature electrostatic levitator: density, volume expansion, specific heat capacity, emissivity, surface tension and viscosity. *Journal of Crystal Growth* **208**, 313–321 (2000).